1-9-2023

Modulation of RNA splicing enhances response to BCL2 inhibition in leukemia.

Eric Wang

Jose Mario Bello Pineda

Won Jun Kim

Sisi Chen

Jessie Bourcier

See next page for additional authors

Authors

Eric Wang, Jose Mario Bello Pineda, Won Jun Kim, Sisi Chen, Jessie Bourcier, Maximilian Stahl, Simon J Hogg, Jan Phillipp Bewersdorf, Cuijuan Han, Michael E Singer, Daniel Cui, Caroline E Erickson, Steven M Tittley, Alexander V Penson, Katherine Knorr, Robert F Stanley, Jahan Rahman, Gnana Krishnamoorthy, James A Fagin, Emily Creger, Elizabeth McMillan, Chi-Ching Mak, Matthew Jarvis, Carine Bossard, Darrin M Beaupre, Robert K Bradley, and Omar Abdel-Wahab

Cancer Cell

Article

Modulation of RNA splicing enhances response to BCL2 inhibition in leukemia

Graphical abstract

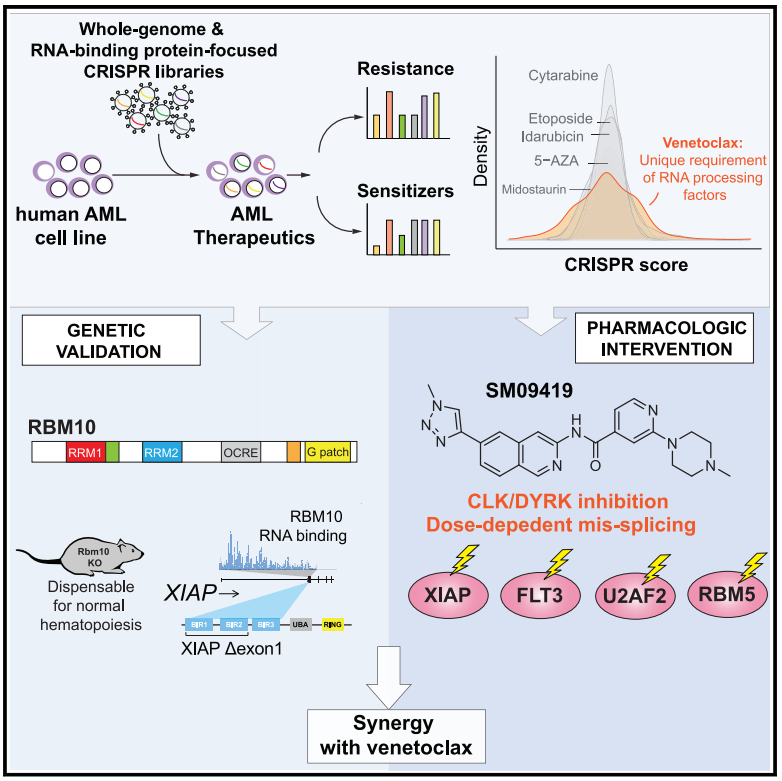

Highlights

- Genome-wide screens identify genomic determinants of drug response in AML
- RBM10 loss enhances venetoclax efficacy and is dispensable for hematopoiesis
- Inhibition of splicing-dependent kinases overcomes venetoclax resistance
- SM09419 synergizes with venetoclax by impairing XIAP and splicing factors

Authors

Eric Wang, Jose Mario Bello Pineda, Won Jun Kim, ..., Darrin M. Beaupre, Robert K. Bradley, Omar Abdel-Wahab

Correspondence

eric.wang@jax.org (E.W.),
rbradley@fredhutch.org (R.K.B.),
abdelwao@mskcc.org (O.A.-W.)

In brief

Wang et al. perform genetic screens to identify mediators of sensitization and resistance to acute myeloid leukemia therapies. This reveals a unique relationship between expression of RNA splicing factors and response to the BCL2 inhibitor venetoclax, as well as an inhibitor of splicing-dependent kinases, which overcomes venetoclax resistance.

Wang et al., 2023, Cancer Cell *41*, 164–180
January 9, 2023
https://doi.org/10.1016/j.ccell.2022.12.002

CellPress

CellPress
OPEN ACCESS

Cancer Cell

Article

Modulation of RNA splicing enhances response to BCL2 inhibition in leukemia

Eric Wang,[1,10,*] Jose Mario Bello Pineda,[2,3,4,10] Won Jun Kim,[5,10] Sisi Chen,[5] Jessie Bourcier,[5] Maximilian Stahl,[6] Simon J. Hogg,[5] Jan Phillipp Bewersdorf,[5] Cuijuan Han,[1] Michael E. Singer,[5] Daniel Cui,[5] Caroline E. Erickson,[5] Steven M. Tittley,[5] Alexander V. Penson,[5] Katherine Knorr,[5] Robert F. Stanley,[5] Jahan Rahman,[5] Gnana Krishnamoorthy,[7,8] James A. Fagin,[7,8] Emily Creger,[9] Elizabeth McMillan,[9] Chi-Ching Mak,[9] Matthew Jarvis,[9] Carine Bossard,[9] Darrin M. Beaupre,[9] Robert K. Bradley,[2,3,*] and Omar Abdel-Wahab[5,11,*]

[1]The Jackson Laboratory for Genomic Medicine, Farmington, CT 06032, USA
[2]Public Health Sciences and Basic Sciences Divisions, Fred Hutchinson Cancer Research Center, Seattle, WA, USA
[3]Department of Genome Sciences, University of Washington, Seattle, WA, USA
[4]Medical Scientist Training Program, University of Washington, Seattle, WA, USA
[5]Molecular Pharmacology Program, Sloan Kettering Institute, Memorial Sloan Kettering Cancer Center, New York, NY, USA
[6]Department of Medical Oncology, Dana-Farber Cancer Institute, Boston, MA, USA
[7]Human Oncology and Pathogenesis Program, Memorial Sloan Kettering Cancer Center, New York, NY, USA
[8]Department of Medicine, Division of Endocrinology, Memorial Sloan Kettering Cancer Center, New York, NY, USA
[9]Biosplice Therapeutics Inc., San Diego, CA, USA
[10]These authors contributed equally
[11]Lead contact
*Correspondence: eric.wang@jax.org (E.W.), rbradley@fredhutch.org (R.K.B.), abdelwao@mskcc.org (O.A.-W.)
https://doi.org/10.1016/j.ccell.2022.12.002

SUMMARY

Therapy resistance is a major challenge in the treatment of cancer. Here, we performed CRISPR-Cas9 screens across a broad range of therapies used in acute myeloid leukemia to identify genomic determinants of drug response. Our screens uncover a selective dependency on RNA splicing factors whose loss preferentially enhances response to the BCL2 inhibitor venetoclax. Loss of the splicing factor RBM10 augments response to venetoclax in leukemia yet is completely dispensable for normal hematopoiesis. Combined RBM10 and BCL2 inhibition leads to mis-splicing and inactivation of the inhibitor of apoptosis *XIAP* and downregulation of *BCL2A1*, an anti-apoptotic protein implicated in venetoclax resistance. Inhibition of splicing kinase families CLKs (CDC-like kinases) and DYRKs (dual-specificity tyrosine-regulated kinases) leads to aberrant splicing of key splicing and apoptotic factors that synergize with venetoclax, and overcomes resistance to BCL2 inhibition. Our findings underscore the importance of splicing in modulating response to therapies and provide a strategy to improve venetoclax-based treatments.

INTRODUCTION

Acute myeloid leukemia (AML) is an aggressive hematologic malignancy marked by a dismal prognosis.[1] For decades, the standard therapy for newly diagnosed AML has been intensive cytotoxic chemotherapy. Recently, several targeted therapies have been approved for AML, including inhibitors of IDH1/2, FLT3, and BCL2.[2] Despite the introduction of these agents, most patients ultimately relapse and acquire resistance to long-term, continuous drug exposure.[3,4] Genetic mutations, such as in TP53, have been shown to contribute to poor prognosis in patients treated with chemotherapy or the BCL2 inhibitor venetoclax.[5–7] More recently, acquired BAX mutations have been shown to confer resistance to venetoclax in a subset of AML patients.[8] However, in the majority of cases, genetic lesions are not known to be the main underlying mechanism of AML relapse,[9,10] possibly implicating non-genetic mechanisms that allow persistent survival of leukemia cells on exposure to drug therapy.[11] For instance, upregulation of anti-apoptotic proteins[12,13] and dysregulated mitochondrial metabolism[14–16] can alter responsiveness to venetoclax. Such findings have demonstrated that epigenetic plasticity and transcriptional variability can act as critical evolutionary drivers of clonal fitness and drug resistance in leukemia.[17,18]

Combinatorial therapies have been widely used to circumvent acquired drug resistance and as an approach with proven clinical efficacy for the treatment of several cancer types.[19,20] In AML, the combination of venetoclax with hypomethylating agents is now widely used and has significantly improved the response and survival rates of patients.[21,22] However, despite the success of venetoclax and hypomethylating agent combination therapy, this regimen is not curative. Furthermore, the majority of patients are unable to undergo curative allogeneic stem cell transplantation and ultimately become resistant to therapy.[22] As such, identifying and targeting drug-resistance

mechanisms in AML with combinatorial treatment regimens is of critical importance.

Here, we utilized unbiased genetic screens to map drug/gene interactions for a variety of clinically approved therapies used in the treatment of AML. This effort highlighted a unique genetic relationship between response to venetoclax and the function of specific RNA splicing factors. Although there is a well-established role for RNA splicing in the regulation of apoptosis,[23] clinically viable means to manipulate splicing to enhance cell death in cancer have been limited to date. As genetic proof of concept, we identified a number of splicing factors whose loss promotes cell death in the setting of venetoclax and that are dispensable for normal hematopoiesis, suggesting a therapeutic index for augmenting venetoclax response by modulating RNA splicing. Moreover, we present a compound to modulate RNA splicing and enhance venetoclax response via inhibition of the splicing kinase families known as CLKs (CDC-like kinases) and DYRKs (dual-specificity tyrosine-regulated kinases).

RESULTS

Mapping genomic determinants of AML drug response

To explore drug-gene interactions that underpin response to AML therapies, we performed a genome-wide Clustered Regularly Interspaced Short Palindromic Repeats (CRISPR) screen containing 77,441 single guide RNAs (sgRNAs) targeting 19,115 genes.[24] We transduced this library into the human AML cell line, MOLM-13 (an MLL-AF9 translocated cell line bearing a concomitant *FLT3*^{ITD} mutation) and after 8 days post-transduction, cells were treated with a broad range of clinically approved AML drugs (venetoclax, 5-azacytidine, cytarabine, etoposide, midostaurin, and idarubicin) (Figure 1A). Changes in sgRNA abundance were assessed at day 20 post-transduction by measuring the average fold change (drug/DMSO) of all sgRNAs targeting a given gene, and top scoring candidates were classified as genes that sensitize (negative CRISPR score) or confer resistance (positive CRISPR score) to individual drugs (Table S1).

We identified previously characterized genes shown to mediate resistance to these compounds, including sgRNAs targeting the pro-apoptotic factors, *BAX* and *PMAIP* (also known as *NOXA*), as well as *TP53* to confer venetoclax resistance[5] (Figure 1B). We also confirmed that inactivation of *TOP2A*, a target of etoposide, promoted survival of AML cells against etoposide exposure. Of note, sgRNAs targeting the uridine-cytidine kinase *UCK2* scored as the top positive hit in our 5-azacytidine screen, and UCK has been previously implicated to confer resistance to the hypomethylating agent.[25,26]

To identify combinatorial strategies that enhance existing AML therapies, we explored genes whose sgRNAs were significantly depleted on drug exposure. We performed Gene Ontology (GO) enrichment analysis on the top scoring negative hits from each CRISPR screen and uncovered significant terms associated with RNA splicing and regulation of mRNAs, linked to venetoclax sensitization (Figure 1C). Consistently, we observed a significantly wider distribution (higher variance) of CRISPR scores for sgRNAs targeting RNA processing genes in the setting of venetoclax treatment compared with other drugs (Figure S1A). These data suggest a unique relationship between perturbation of RNA processing and response to venetoclax compared with other commonly used AML therapies. Previous reports have indicated the importance of leukemia cells exploiting alternative splicing and post-transcriptional mechanisms to promote tumor growth and therapy resistance.[27–31] Moreover, clinical observations in AML patients have also demonstrated correlations between spliceosome mutations and alterations in response to venetoclax.[6,32]

To further investigate the functional impact of RNA splicing factors in modulating drug response, we applied a previously developed CRISPR library targeting functional domains of 492 RNA-binding proteins (RBPs) consisting of 2,855 sgRNAs[27] to enhance CRISPR-Cas9 negative selection by targeting functional protein domains[33] (Figure 1D). Consistent with our initial findings from the genome-wide screen, we identified that loss-of-function of several RNA splicing factors enhanced sensitivity or resistance to venetoclax treatment (Figures 1E and 1F). We further validated the top scoring sensitizers, such as *RBM10*, *SRSF11*, *SRSF8*, *HNRNPD*, *HNRNPAB*, and *HNRNPF*, whose inactivation led to preferential sensitivity in AML cells treated with venetoclax, which was not seen with other tested therapeutics (Figures 1G and S1B–S1D).

Loss of RBM10 sensitizes leukemia cells to venetoclax

Among the top gene candidates whose loss sensitized cells to venetoclax was RBM10, whose loss-of-function exclusively enhanced venetoclax efficacy in AML among other drugs screened (Figures 1F, 1G, and S2A). We further explored publicly available genome-wide CRISPR screens performed in a broad range of human cancer cell lines, which revealed that *RBM10* loss is least essential in leukemia cell lines compared with other cancer subtypes (Figure S2B). However, in the presence of venetoclax, RBM10 deletion strikingly conferred preferential lethality and anti-leukemic effects in human AML cell lines across a variety of molecular subtypes (Figures 2A–2C and S2C). Of note, RBM10 deletion even augmented BCL2 inhibition in TP53-mutated AML cell lines (THP-1 and U937),[34] which have been previously described as venetoclax resistant[5,6] (Figure S2D).

We next assessed the impact of RBM10 deletion on the response of human AML cells to venetoclax *in vivo*. To achieve this, we transplanted MOLM-13 cells stably expressing firefly luciferase and anti-RBM10 sgRNAs or the non-targeting control (sgRosa) into non-obese diabetic (NOD)/severe combined immunodeficiency (SCID) IL2Rgamma^{null} (NSG) mice. On disease onset, mice were treated with venetoclax (100 mg/kg/day) or vehicle control (Figure 2D). Consistent with our *in vitro* findings, RBM10 deletion reduced leukemia burden and extended survival in the setting of venetoclax treatment (Figures 2E, 2F, and S2E). Indel analysis of prolonged RBM10 sgRNA editing by next-generation sequencing showed an outgrowth of cells containing in-frame RBM10 mutations, implicating that mice succumb to an outgrowth of sgRNA-expressing cells that retain RBM10 functionality (Figure S2F). Overall, these findings provide genetic evidence that loss of RBM10 has a synthetic lethal relationship with BCL2 inhibition in AML.

Many RNA splicing factors are known to be pan-essential for cell survival.[35] To evaluate the therapeutic potential of RBM10 modulation as a therapeutic candidate for venetoclax-based therapies, we generated an Rbm10 conditional knockout (KO; cKO) mouse by inserting *loxP* sites flanking exon 3 of *Rbm10* (*Rbm10*$^{fl/fl}$; Figure 2G) and crossing with interferon-induced *Mx1*-driven Cre

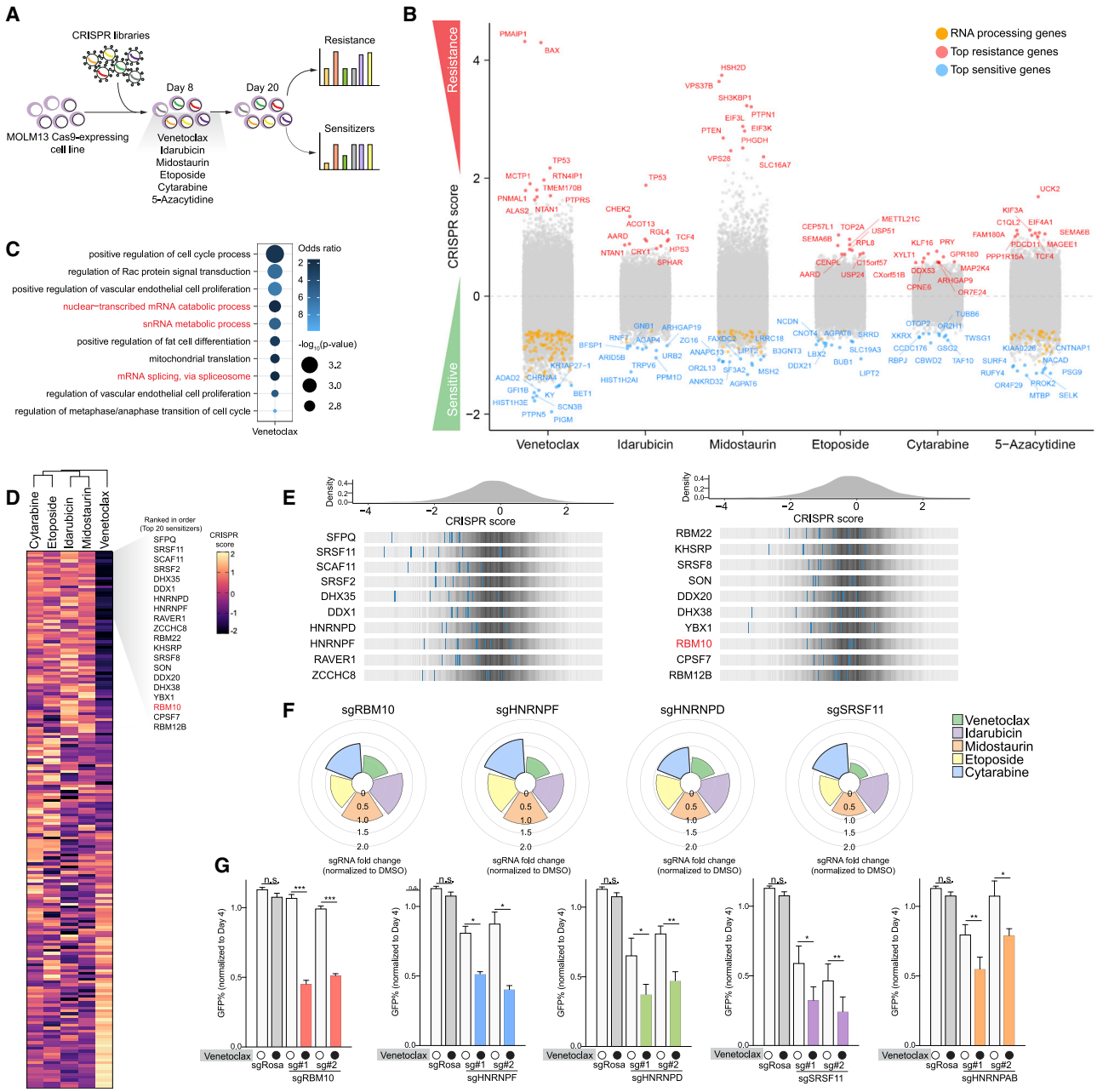

Figure 1. Mapping genomic determinants of AML drug response and synthetic lethal relationship between RNA splicing factors and venetoclax sensitivity

(A) Schematic of genome-wide CRISPR screens in MOLM-13 AML cells treated with a panel of clinically approved AML drugs.

(B) Manhattan plot depicting top 10 genes that sensitize (blue) or confer resistance (red) in individual CRISPR drug screens. Orange dots represent RNA processing genes. CRISPR score represents the log2 (fold-change) values of sgRNAs normalized to DMSO.

(C) Gene Ontology (GO) enrichment analysis of top sensitizers in the venetoclax screen.

(D) Clustered heatmap of results of the RNA-binding protein-focused CRISPR drug screens in MOLM-13 AML cells treated with drugs. CRISPR score represents log2 fold change of sgRNAs normalized to DMSO.

(E) Histogram of CRISPR scores for all sgRNAs in the venetoclax screen in (D). Values represent the log2 (fold-change) values of sgRNAs normalized to DMSO. The blue lines represent individual sgRNAs targeting the indicated genes among the top splicing factor candidates.

(F) Polar plots of top synergistic splicing factors identified in (D) treated with various AML drugs. The height of the wedge corresponds to the sgRNA fold change normalized to DMSO.

(G) Competition-based assay in MOLM-13 cells 10 days post-transduction with top two sgRNAs targeting each splicing factor or non-targeting sgRosa control (n = 3 per condition; mean + SEM) treated with 50 nM venetoclax.

Statistical analysis was performed using unpaired Student's *t* test by Prism GraphPad (*p < 0.05, **p < 0.01, ***p < 0.001). n.s., not significant. See also Figure S1 and Table S1.

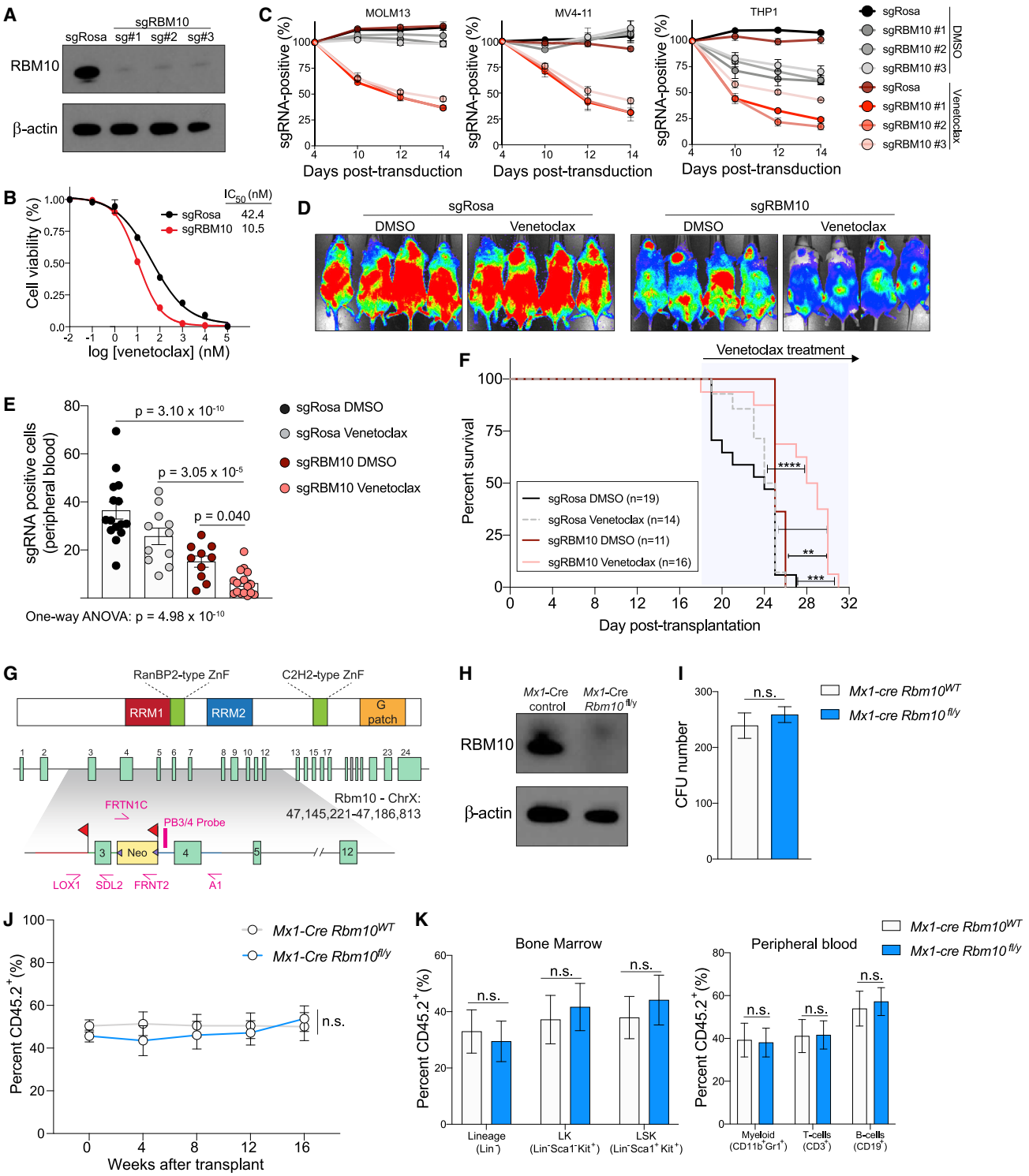

Figure 2. RBM10 loss enhances BCL2 inhibition in AML cells but is dispensable for normal hematopoiesis

(A) Western blot of CRISPR-mediated knockout (KO) of RBM10 in MOLM-13 cells.

(B) Dose-response curves of sgRBM10 or sgRosa treated with indicated venetoclax concentrations on the x axis and cell viability on the y axis at 48 h. IC_{50} values were calculated from technical triplicates per experiment; error bars represent SEM.

(C) Competition proliferation assays of sgRBM10 or non-targeting sgRosa in human AML cell line expressing Cas9 and treated with 50 nM venetoclax or DMSO (n = 3 biological replicates per time point and condition; mean + SEM).

(legend continued on next page)

recombinase mice. Following intraperitoneal polyinosinic-polycytidylic acid (pIpC) injections, Rbm10 cKO mice were confirmed to excise exon 3 of *Rbm10*, leading to an early frameshift and loss of Rbm10 protein in bone marrow cells (Figures 2H, S2G, and S2I). We next assessed stem cell functionality using *in vitro* colony-replating assays, which demonstrated that Rbm10 deletion in hematopoietic precursors did not impair colony formation (Figure 2I). In parallel, bone marrow-derived cells from CD45.2$^+$ *Rbm10* floxed mice were transplanted in a competitive manner along with competitor *Rbm10* wild-type CD45.1$^+$ cells and treated with pIpC after stable reconstitution of hematopoiesis. There was no significant effect of Rbm10 deletion on absolute numbers or frequency of peripheral blood and bone marrow cells (Figures 2J, 2K, S2J, and S2K). These data demonstrate that Rbm10 is dispensable for normal hematopoiesis.

Dual inhibition of RBM10 and BCL2 promotes *XIAP* mis-splicing

We next sought to understand the mechanistic basis for the relationship between RBM10 loss and enhanced response to venetoclax. The effects of RBM10 KO on venetoclax response were rescued by expressing an *RBM10* cDNA impervious to anti-RBM10 sgRNAs (because of mismatches between cDNA sequence and the RBM10 sgRNAs; Figure 3A). However, expression of RBM10 lacking its second RNA recognition motif 2 (RRM2) or C2H2-type zinc finger (C2H2 ZnF)[36] failed to rescue response to venetoclax (Figure 3A).

The above data indicate the importance of RBM10's RNA-binding domains on venetoclax response. We therefore further assessed the direct impact of RBM10-RNA interactions on pre-mRNA binding and splicing, which have not been explored in hematopoietic cells previously. We performed anti-RBM10 enhanced UV cross-linking immunoprecipitation (eCLIP)[37] in MOLM-13 AML cells (Figure S3A). This approach identified approximately 29,000 significant sequence clusters bound by RBM10, which corresponded to ~5,000 annotated transcripts (Table S2). Approximately 90% of RBM10 binding sites mapped to intronic sites, with a preferential occupancy of distal (farther than 500 nt from the splice-site region) (77.1%) and proximal (within 500 nt of the splice-site region) intronic (8%) sequences near 5′-AND-3′ splice sites throughout the transcriptome (Figures 3B and S3B).

Next, we evaluated the transcriptional and splicing changes in RBM10-deleted AML cells treated with venetoclax or DMSO, compared with non-targeting sgRosa, by RNA sequencing (RNA-seq) (Tables S3 and S4). We measured isoform usage frequencies across seven main types of alternative splicing event (skipped [or retained] cassette exons [SEs], alternative 5′ splice sites [A5SSs], alternative 3′ splice sites [A3SSs], mutually exclusive exons [MXEs], tandem 3′ UTRs [TUTRs], and retained [RIs] and constitutive introns [CIs]) to quantify splicing changes across treatments (Figures S3C and S3D). RBM10 KO primarily led to changes in cassette exon splicing (Figure 3C), suggesting that RBM10 most commonly regulates exon usage in AML cells. In comparison, RBM10 deletion in the presence of venetoclax amplified the degree of aberrant splicing involving CIs and cassette exons. Most notably, we observed an increase in exon exclusion events in the combination treatment versus RBM10 deletion alone (n = 342) (Figure 3D).

We further investigated the link between RBM10 binding and differential splicing observed in combined RBM10 KO and venetoclax. These analyses revealed *RBM10* binding signal in the 5′ region of the upstream intron of repressed cassette exons following combination treatment, suggestive of a role of RBM10 binding in this region in promoting exon exclusion (Figure 3E). Interestingly, we found that the inhibitor of apoptosis protein (IAP) family member, *XIAP*, displayed increased exclusion of the first coding exon in venetoclax-treated RBM10 KO AML cells, which also had significant RBM10 binding at this region (Figures 3F and S3E). *XIAP*, also known as *BIRC4*, binds and sequesters pro-apoptotic caspases through direct protein-protein interactions with its BIR domains to prevent caspase homodimerization, thereby inactivating apoptosis.[38–41] Based on our findings, we hypothesize that activation of apoptosis is a consequence of skipping the first coding exon of *XIAP*. The resulting mRNA lacks *XIAP*'s canonical start codon, as well as the sequence encoding the majority of its BIR1-3 domains, strongly suggesting that this splicing change results in loss of functional *XIAP* production (Figure 3G). We also functionally evaluated the mis-spliced isoform of *XIAP* event induced by *RBM10* KO and venetoclax treatment (which we refer to as *XIAP* Δexon 1) by ectopically expressing full-length *XIAP* (FL) or *XIAP* Δexon 1 linked to a GFP reporter in MOLM-13 cells (Figure 3H). Consistent with the function of IAP proteins, we found *XIAP* FL

(D) Bioluminescent imaging of mice transplanted with MOLM-13 cells transduced with sgRBM10 or sgRosa and treated daily with venetoclax (100 mg/kg) or vehicle control. Representative images of four mice per condition are shown. Images were taken 4 days post-treatment.
(E) Flow cytometry analysis of GFP-positive sgRNA-expressing, indicated by y axis, MOLM-13 cells in peripheral blood at day 6 post-treatment. Statistical analysis was performed using one-way ANOVA with *post hoc* testing as indicated (number of mice used in each group is indicated in F; mean + SEM).
(F) Kaplan-Meier survival curves of mice transplanted with MOLM-13 cells transduced with sgRBM10 or sgRosa and treated daily with venetoclax (100 mg/kg) or vehicle. The p values were determined using a log rank Mantel-Cox test (**p < 0.01, ***p < 0.001).
(G) Schematic depiction of the targeting strategy to generate Rbm10 cKO mice. The Rbm10 allele was deleted by targeting exon 3 that resulted in a frameshift following excision. Two *LoxP* sites flanking exon 3 and an Frt-flanked neomycin selection cassette were inserted in the downstream intron.
(H) Western blot of Rbm10 in bone marrow mononuclear cells from Mx1-cre Rbm10 fl/y (Rbm10 cKO) or Mx1-cre control 7 days after polyinosinic-polycytidylic acid (pIpC) treatment.
(I) Total number of colony-forming units (CFUs) from bone marrow cells of Mx1-cre Rbm10 fl/y (Rbm10 cKO) or Mx1-cre control mice following 7 days of culture (n = 6; mean + SEM). The p values were determined by unpaired Student's *t* test.
(J) Percentage of CD45.2$^+$ cells in peripheral blood over the course of 4 months of competitive transplantation (n = 6 for Mx1-cre control and n = 7 mice for Rbm10 cKO; mean + SEM).
(K) Percentage of CD45.2$^+$ hematopoietic stem and progenitor cells in the bone marrow (left) and mature immune cells in the peripheral blood (right) (n = 6 for Mx1-cre control and n = 7 mice for Rbm10 cKO; mean + SEM).
See also Figure S2.

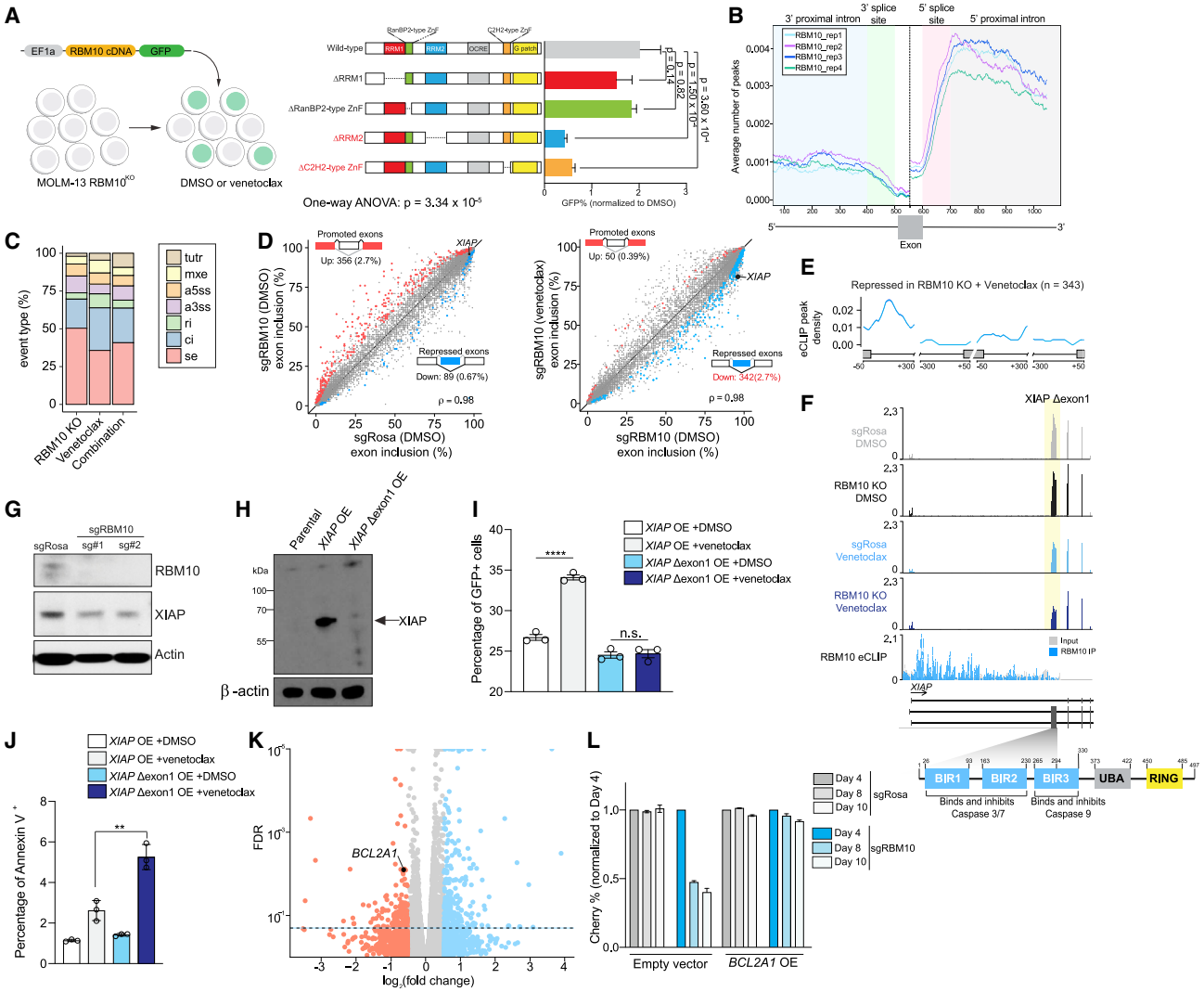

Figure 3. Impact of RBM10 on RNA binding, RNA splicing, and response to venetoclax

(A) Competition-based assay of RBM10 KO in MOLM-13 cells and transduced with *RBM10* cDNA wild-type (WT) or individual mutant (lacking RNA-binding domains) *RBM10* cDNA and treated with venetoclax (50 nM) or DMSO at 48 h (n = 3; mean + SEM). The p values were determined by one-way ANOVA with *post hoc* testing.

(B) Metaintron plots of average number indicated by y axis of RBM10 peaks mapped to intronic regions flanking exons in MOLM-13 cells (n = 4 eCLIP replicates). This plot is exon centered (500–600 bp) on the x axis. Enhanced cross-linking and immunoprecipitation (eCLIP) was performed in four replicates.

(C) Percentage of treatment-responsive (RBM10 KO, venetoclax, or RBM10 KO and venetoclax) differentially spliced event types: cassette exons (SEs), alternative 5′ splice site (ss) exon (A5E), alternative 3′ ss exon (A3E), mutually exclusive exons (MXEs), retained intron (RI), constitutive intron (CI), and tandem 3′ UTR (TUTR) from RNA-seq (n = 3 per condition).

(D) Scatterplot of SEs promoted (red circles) or repressed (blue circles) in MOLM-13 cells transduced with sgRosa (y axis) or sgRBM10 (x axis) treated with DMSO or venetoclax RNA-seq (n = 3 per condition). ρ denotes Spearman's rank correlation coefficient.

(E) RBM10 splicing map generated by integrating RBM10 KO splicing changes from RNA-seq and RBM10 eCLIP binding sites.

(F) RNA-seq and eCLIP (bottom) coverage plots of XIAP Δexon1 in MOLM-13 cells with RBM10 KO or non-targeting sgRNAs treated with DMSO or venetoclax. Yellow shadow depicts exon exclusion event in RBM10KO venetoclax-treated MOLM-13 cells overlapped with functional protein domains of XIAP.

(G) Western blotting of XIAP after 50 nM venetoclax treatment of MOLM-13 cells with sgRosa or sgRBM10 for 48 h.

(H) Western blotting of XIAP protein levels after ectopic overexpression of XIAP full-length (FL) or XIAP Δexon1.

(I) Competition-based assay of XIAP FL or XIAP Δexon1 linked to GFP reporter after 24 h of venetoclax treatment (n = 3; mean + SEM). y axis denotes GFP-positive cells.

(J) Annexin V staining of *XIAP* FL or *XIAP* Δexon1 after 24 h of venetoclax treatment (n = 3; mean + SEM). y axis denotes Annexin V-positive cells. Statistical analysis was performed using unpaired Student's *t* test by Prism GraphPad (*p < 0.05, **p < 0.01).

(K) Volcano plot of differentially expressed genes (DEGs) on RBM10KO venetoclax-treated MOLM-13 cells compared with DMSO RNA-seq (n = 3 per condition).

(L) Competition-based assay measuring Cherry-expressing sgRBM10 or sgRosa cells transduced with overexpression (OE) of *BCL2A1* cDNA or empty vector GFP-positive cells in MOLM-13 cells treated with 50 nM venetoclax for 48 h (n = ; mean + SEM). y axis denotes mCherry-positive cells.

See also Figure S3 and Tables S2, S3, and S4.

overexpression allowed survival of AML cells after venetoclax treatment, whereas *XIAP* Δexon 1 resulted in increased apoptosis (Figures 3I, 3J, and S3F). Overall, these results demonstrate that XIAP Δexon 1 cannot rescue cell death induced by venetoclax treatment and RBM10 deletion (Figure S3G). Importantly, prior work has demonstrated that inhibition of *XIAP* synergized with venetoclax,[42] highlighting the importance of *XIAP* levels in BCL2 inhibitor sensitivity.

Gene expression analysis of venetoclax-treated *RBM10* KO AML cells revealed downregulated expression of *BCL2A1*, which encodes an anti-apoptotic factor whose expression is correlated with venetoclax resistance in AML patients[6,43] (Figures 3K, S3H, and S3I). Consistent with these data, overexpression of *BCL2A1* cDNA was able to fully rescue the anti-leukemic effects seen with the combined loss of *RBM10* and *BCL2* inhibition (Figure 3L). Moreover, we did not observe significant RBM10 eCLIP peaks or splicing alteration of *BCL2A1* mRNA, which suggests that upstream factors may regulate *BCL2A1* transcript. Overall, these data provide mechanistic evidence that the combined loss of RBM10 and BCL2 leads to altered splicing and expression of mRNAs encoding key apoptotic genes.

Pharmacologic inhibition of splicing kinases synergizes with venetoclax

Utilizing our CRISPR screens to identify pharmacologically intervenable splicing factors to augment venetoclax response, we found that inactivation of several serine/arginine (SR)-rich proteins (*SRSF2*, *SRSF3*, *SRSF8*, and *SRSF11*) sensitized AML cells to venetoclax (Figure 1D; Table S1). The family of SR splicing factors is essential for alternative pre-mRNA splicing, and their activity is tightly regulated by post-translational modifications placed by serine/threonine kinases.[44–46] For example, CLKs phosphorylate arginine/serine (RS) domains in SR proteins and regulate pre-mRNA splicing.[45,47] Moreover, DYRK1A has been reported to regulate alternative splicing via phosphorylation of SF3B1.[48–50] In addition, analysis of publicly available genome-wide CRISPR screens from DepMap[51] revealed *BCL2* as one of the top co-dependencies with DYRK1A loss (Figure S4A).

These findings support the rationale to inhibit splicing-dependent kinases as a combinatorial strategy with venetoclax treatment. To pursue therapeutic inhibition of splicing-dependent kinases, we developed SM09419, a pan-CLK pan-DYRK inhibitor, via rational design and iterative medicinal chemistry to achieve drug-like and favorable pharmacokinetic profiles (Figures 4A–4D). We confirmed the selectivity of SM09419 to target CLK1–4, as well as DYRK1A-B and DYRK2, using in-cell NanoBRET target engagement assays (Figures 4C and S4B). Accordingly, SM09419 treatment resulted in dose-dependent reduction of CLK activity and SR protein phosphorylation in AML cells (Figures 4E and S4C). Next, we assessed the combinatorial effects of SM09419 with a panel of drugs (venetoclax, 5-azacytidine, cytarabine, and midostaurin) in human AML cell lines. We observed a synergistic effect exclusively when combining SM09419 and venetoclax in MOLM-13 parental and venetoclax-resistant cells, but not with other drugs (Figures 4F–4I, S4D, and S4E). Despite robust anti-leukemic effects of SM09419 *in vitro*, SM09419 (25 mg/kg) treatment in wild-type C57BL/6 mice was well tolerated *in vivo* with no signs of hematologic toxicities (based on serial blood counts, *in vitro* hematopoietic progenitor cell assays, and detailed analysis of hematopoietic cell composition in blood and bone marrow) or liver or kidney dysfunction, thus providing a rationale for pharmacologic inhibition of CLK/DYRK in combination with venetoclax in AML (Figures S5A–S5H).

To understand the mechanistic basis for the synergy of SM09419 and venetoclax combination, we performed RNA-seq on MOLM-13 human AML cells treated with SM09419 alone or in combination with venetoclax (Tables S5 and S6). Splicing analyses showed that SM09419 alone, or in combination with venetoclax, mainly resulted in changes in the processing of CIs/RIs and cassette exons (Figure 5A). CLK/DYRK inhibition affects cassette exon recognition in a sequence-specific manner, as evidenced by the enrichment of pyrimidines in exons preferentially excluded on SM09419 treatment (Figure 5B). Although venetoclax monotherapy had no significant effects on RNA splicing, treatment with SM09419 or the combination resulted in striking reductions in RNA splicing efficiency as manifested by cassette exon skipping and intron retention (Figures 5A and 5C; Table S6). Of note, these splicing shifts resulted in substantial increases in levels of mRNAs that contain premature termination codons and are therefore predicted substrates for degradation by nonsense-mediated decay (NMD).

In order to understand how the effects of SM09419 relates to deletion of RBM10, we next performed a systematic comparison of the splicing changes and gene expression across both conditions in the same MOLM-13 cells. Both RBM10 deletion and SM09419 treatment cause splicing changes that promote NMD-inducing transcripts. However, the magnitude of NMD-inducing splicing events is greater with SM09419 treatment (a result consistent with the fact that RBM10 deletion in the absence of any drug treatment is well tolerated in MOLM-13 cells) (Figure 5D). Nonetheless, a number of mRNA isoforms were shared across RBM10 deletion versus SM09419 treatment in the absence and presence of concomitant venetoclax treatment. Interestingly, one concordant effect was the same mis-splicing event in *XIAP* seen with RBM10 deletion (Figures 5E and 5F). Finally, both RBM10 deletion and SM09419 treatment prominently downregulate TNFAIP3 (also known as *A20*) (Figure S6A). *TNFAIP3* is a well-described regulator of nuclear factor κB (NF-κB) signaling,[52] and its inhibition may explain the *BCL2A1* downregulation in *RBM10* KO cells exposed to venetoclax. Transcriptomic analysis of SM09419-treated AML cells also demonstrated downregulation of MYB and MYC mRNA levels, which are essential oncogenic factors in AML (Figure S6B).[53,54]

SM09419 induces splicing alterations of key survival genes in AML

Further characterization of SM09419-associated splicing changes revealed increased intron retention within the transcripts of a number of RNA splicing factors (*SRSF5*, *U2AF2*, *RBM17*, and *RBM5*), which also led to decreased protein expression in two independent human AML cell lines (Figures 5G, 5H, and S6C–S6E). Interestingly, several of these same splicing factors were also identified by our CRISPR screens as genes whose inactivation enhanced venetoclax efficacy, which therefore explains the synergistic effects when combining SM09419 and venetoclax (Figures 5E and 5I). Furthermore, we found that SM09419-treated AML cells led to downregulation of several key apoptotic proteins, such as MCL-1, which have been shown to be upregulated in hematologic

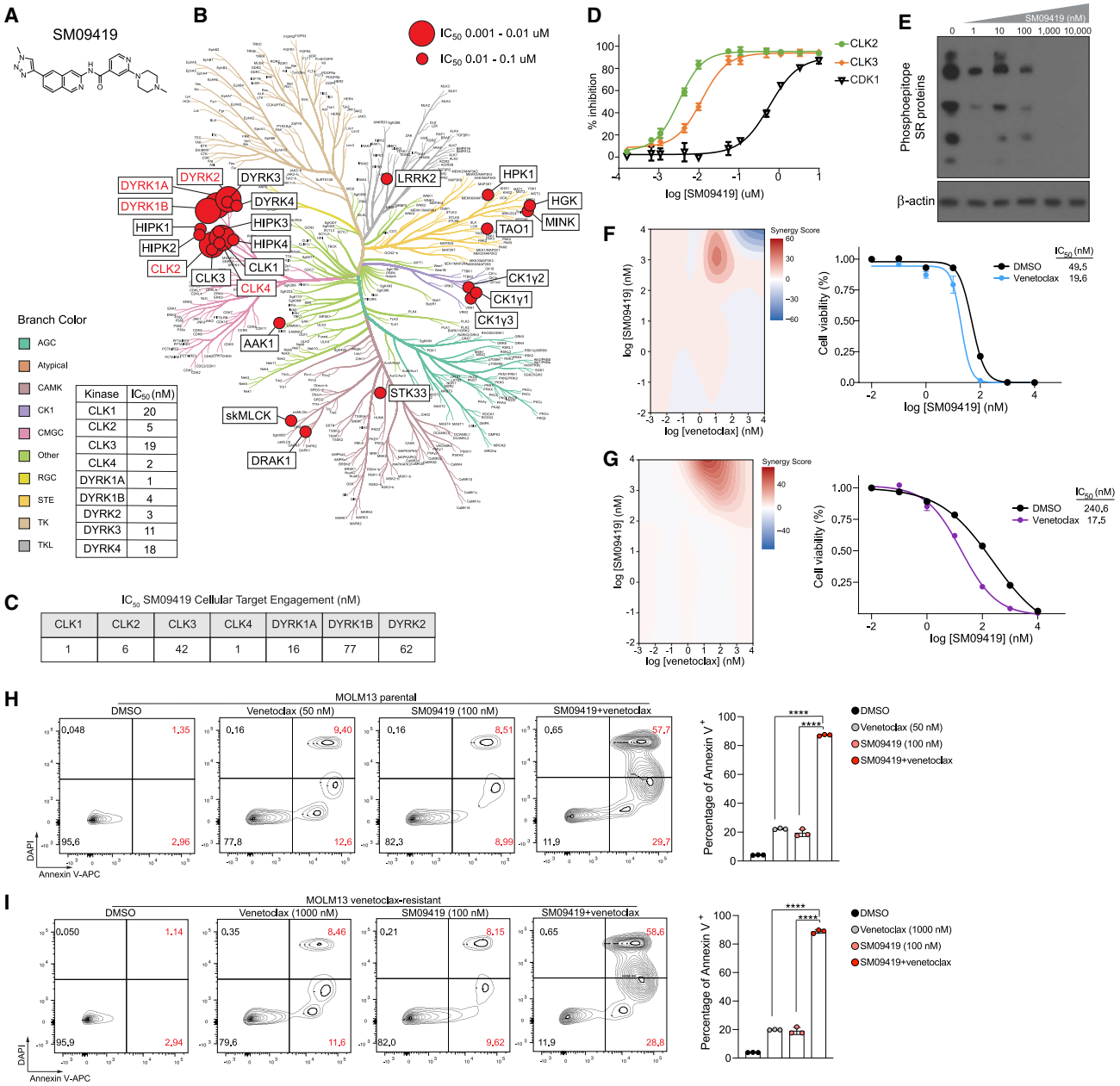

Figure 4. Pharmacologic inhibition of splicing-dependent kinases synergizes with venetoclax

(A) Structure of SM09419 selectivity.

(B) Kinase dendrogram of SM09419. Kinases with IC_{50} values of 0.01–0.1 μM are indicated by small red circles, whereas larger red circles represent more potent IC_{50} values with 0.001–0.01 μM.

(C) NanoBRET target engagement assay of CLK1–4, DYRK1A/B, and DYRK2 on 2 h of SM09419 treatment.

(D) Inhibition of CLKs (CLK2, CLK3, and CDK1) (n = 3). IC_{50} values were determined from dose-response curves. y axis denotes the percent inhibition for CLK2, CLK3, and CDK1 (n = 3; mean + SD).

(E) Western blot of phosphorylated SR proteins treated with increasing concentration of SM09419 for 48 h in MOLM-13 cells.

(F and G) 2D synergy plots using zero interaction potency (ZIP) model (left) and dose-response curves (right) of SM09419 and venetoclax combination at various concentration treated for 48 h in MOLM-13 (n = 3; mean + SEM) and (G) KG-1 cells (n = 3; mean + SEM). The presence of synergy was determined using the SynergyFinder computational package and the ZIP synergy index in which red signifies synergism and blue is antagonism. A positive synergy score is the percent more cell death than expected. IC_{50} values were calculated from technical triplicates per experiment.

(H and I) Annexin V staining (left) and quantification (right) of MOLM-13 (H) parental and (I) venetoclax-resistant cell lines treated with SM09419, venetoclax, or the combination at 48 h post-treatment (n = 3; mean + SEM). y axis denotes percent of Annexin V-positive cells.

Statistical analysis was performed using unpaired Student's *t* test by Prism GraphPad (****p < 0.0001). See also Figures S4 and S5.

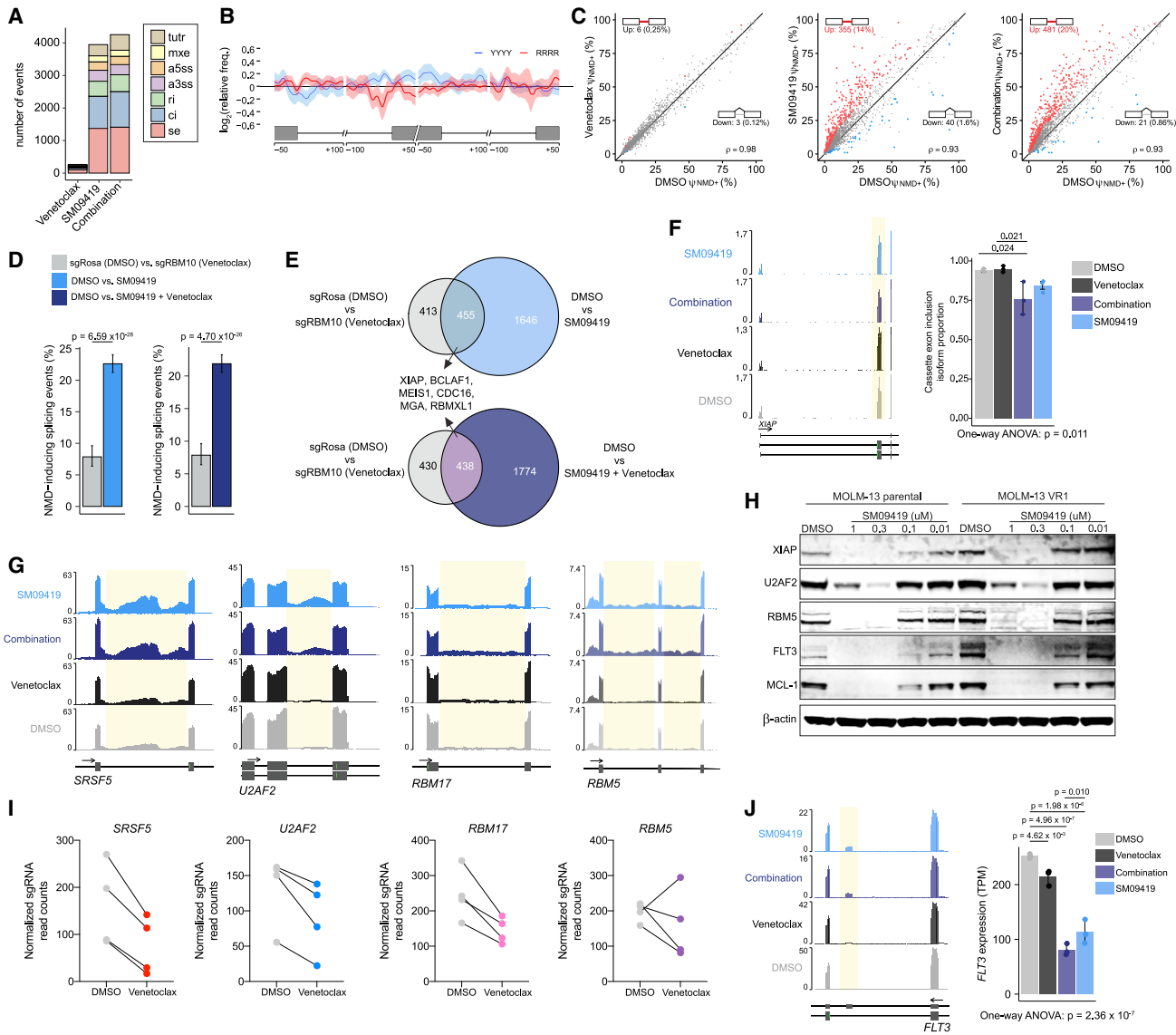

Figure 5. SM09419 promotes mis-splicing of key oncogenic pathways in AML

(A) Total number of splicing changes observed after SM09419 (100 nM), venetoclax (10 nM), or combination of SM09419 (100 nM) and venetoclax (10 nM) treatment for 48-h RNA-seq (n = 3 per condition). SEs, A5E, A3E, MXEs, RI, CI, and TUTR.

(B) Spatial distribution of pyrimidine-rich (YYYY) and purine-rich (RRRR) motifs comparing sequence enrichment of excluded exons (n = 674) against included exons (n = 370) in SM0419-treated (100 nM) MOLM-13 cells.

(C) Scatterplot of NMD-inducing RI events (red circles) in MOLM-13 cells treated with venetoclax (left), SM09419 (middle), or the combination of venetoclax and SM09419 (right) RNA-seq in triplicates for each condition.

(D) Percentage of NMD-inducing events indicated on the y axis in RBM10 KO venetoclax (compared with non-targeting sgRosa) and SM09419, or SM09419 + venetoclax (compared with DMSO) RNA-seq in triplicates for each condition (mean + SEM).

(E) Venn diagram of NMD-inducing events in RBM10 KO venetoclax (compared with non-targeting sgRosa) and SM09419, or SM09419 + venetoclax (compared with DMSO).

(F) RNA-seq coverage plot (left) and mean PSI (Percent Spliced In) of XIAP SE inclusion isoform (n = 3 per condition; mean + SEM).

(G) RNA-seq coverage plots of the splicing factors *SRSF5*, *U2AF2*, *RBM17*, and *RBM5* in MOLM-13 cells. Yellow regions represent RI events in each of the genes.

(H) Western blotting of XIAP, U2AF2, RBM5, FLT3, MCL-1, and actin in MOLM-13 parental or venetoclax-resistant (VR1) cells treated with varying concentration of SM09419 for 24 h.

(I) Normalized sgRNA counts of top splicing factors from RNA-binding protein CRISPR screen that synergized with venetoclax treatment in MOLM-13 cells.

(J) RNA-seq coverage plots (left) and gene expression (right) plots for *FLT3* mRNA (n = 3 per condition; mean + SEM). p values were determined by one-way ANOVA with *post hoc* testing as indicated.

See also Figure S6 and Tables S5 and S6.

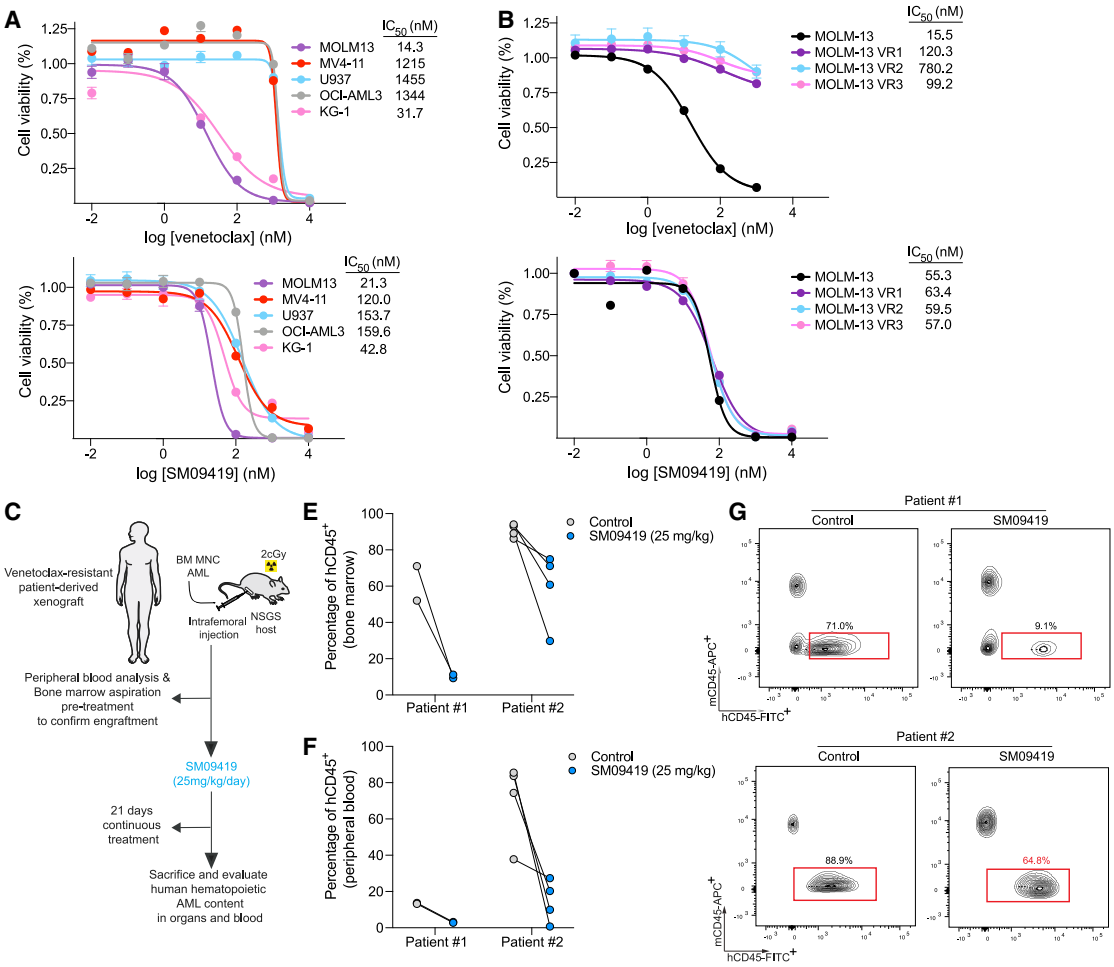

D

Patient	Prior therapies	Reponse	Start of venetoclax	End of venetoclax	Sample date	Genetic alterations
1	VEN+Azacytidine	Primary refractory	01/18/2019	02/27/2019	06/05/2020	RUNX1, PTPN11, FLT3, SF3B1, STAG2
2	VEN+Low-dose Cytarabine	Primary refractory	01/03/2017	04/06/2017	04/10/2017	RUNX1, DNMT3A, IDH2

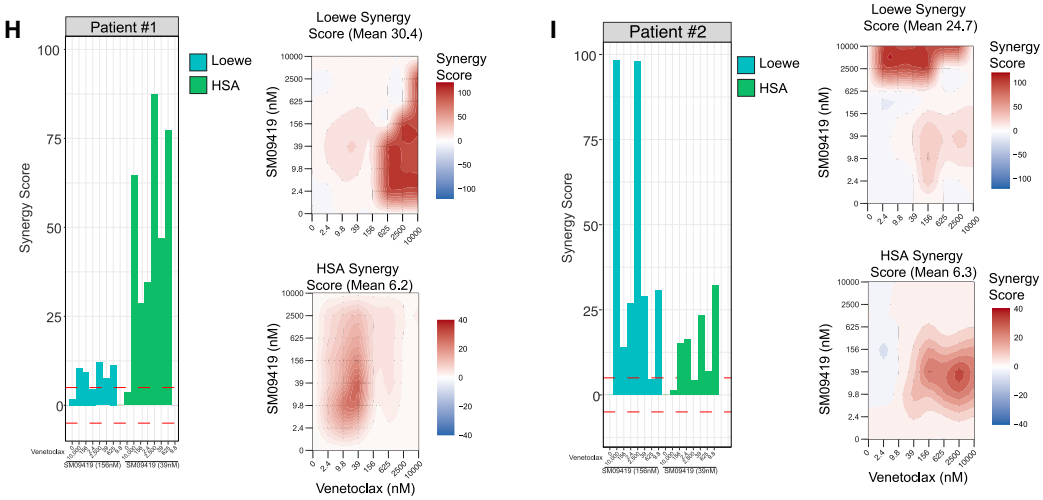

Figure 6. SM09419 circumvents therapeutic resistance to venetoclax

(A) Dose-response curves of human AML cell lines treated with various concentrations of venetoclax (top) or SM09419 (bottom). IC_{50} values were calculated from technical triplicates per experiment; error bars represent SEM.

(legend continued on next page)

neoplasms and confer resistance to BCL2 inhibitors[12] (Figures 5H and S6E). Finally, SM09419 treatment promoted inclusion of an exon with an in-frame stop codon (a "poison exon," whose inclusion renders the transcript NMD sensitive) in the receptor tyrosine kinase FLT3 (Figure 5J). As such, there was reduced *FLT3* mRNA and protein expression in SM09419-treated cells (which is especially pertinent given the known dependence of this FLT3 mutant AML cell line on *FLT3* expression) (Figures 5H and S6E). Importantly, the above results on the impact of SM09419 treatment on XIAP, FLT3, and MCL-1 levels were confirmed in an additional AML cell line. Both venetoclax-resistant and -sensitive KG-1a cells were similarly susceptible to SM09419 treatment and experienced comparable dose-dependent reductions in XIAP, FLT3, and MCL-1 (Figures S6D and S6E).

Additional predicted NMD-inducing splicing events occurred on SM09419 treatment with commensurate reduction in mRNA expression in *SMYD2* (a lysine methyltransferase recognized as a therapeutic target in AML),[53] *DHODH* (a metabolic enzyme and recent AML therapeutic target),[55] *ATAD3A* (a metabolic enzyme whose expression has been included in leukemia stem cell signatures),[56] the MYC target gene *CDC16*,[57] and the additional RNA processing genes *SRPK3*, *TRA2A*, and *DDX51* (Figure S6F). Overall, these data identify that SM09419 downregulates expression of key RNA splicing factors, as well as important apoptotic factors and *FLT3*, via impaired splicing to enhance response to venetoclax in AML while having minimal impact on normal hematopoiesis.

SM09419 overcomes venetoclax-based therapy resistance

We next tested the efficacy of SM09419 across a spectrum of human AML cell lines. SM09419 treatment resulted in broad anti-leukemic effects with potent inhibitory activity across AML subtypes, including cell lines that were highly resistant to venetoclax treatment (Figure 6A). Based on these data, we evaluated the ability of SM09419 to overcome venetoclax resistance. We developed three independent venetoclax-resistant MOLM-13 cell lines following continuous exposure to venetoclax for 3 weeks. Dose-response curves after drug selection confirmed that venetoclax-resistant cell lines displayed a high inhibitory effect concentration ($IC_{50} > 99$ nM) approximately six times greater than parental cells ($IC_{50} = \sim 15$ nM) (Figure 6B). Whole-exome sequencing (WES) and targeted capture sequencing (MSKCC-IMPACT; Memorial Sloan Kettering Cancer Center Integrated Mutation Profiling of Actionable Cancer Targets) did not reveal any known genomic alterations that may cause venetoclax resistance. SM09419 as a single agent led to approximately equally potent inhibitory activity against venetoclax-resistant AML cells as parental, venetoclax-sensitive cells (Figure 6B). Moreover, addition of venetoclax and SM09419 led to synergistic effects in venetoclax-resistant MOLM-13 cells (Figures 4I and S4D). Consistent with our previous findings in MOLM-13 parental cells, we observed downregulation of essential apoptotic proteins (*XIAP*, *MCL-1*), splicing factors (*RBM5*, *U2AF2*), and the tyrosine kinase *FLT3* in venetoclax-resistant MOLM-13 and KG-1a cells (Figures 5H and S6E). We further extended these findings to patient-derived xenograft (PDX) models of AML from patients with *de novo* resistance to venetoclax combination regimens (5-azacytidine or low-dose cytarabine) (Figures 6C and 6D). Following xenotransplantation from two individual venetoclax-resistant patients into NSG-S mice, we detected disease engraftment with $\geq$10% human (h) $CD45^+$ $hCD34^+hCD38^+$ cells and exposed mice to SM09419 (25 mg/kg) or vehicle administered orally and daily for 3 weeks. SM09419 resulted in significant reduction of hCD45 AML cells in the peripheral blood and bone marrow of mice treated with SM09419 when compared with vehicle control (Figures 6D–6F). Moreover, *ex vivo* culturing of these AML patient samples demonstrated single-agent potency of SM09419, as well as synergistic effects when combined with venetoclax (Figures 6G and 6H). Collectively, these findings demonstrate the *in vivo* efficacy of SM09419 to overcome resistance to venetoclax-based therapies.

DISCUSSION

Here, we performed comprehensive mapping of drug-gene interactions that dictate response to a broad range of AML therapies. This effort uncovered genetic strategies that enhance the effects of these existing AML drugs, which may ultimately lead to combinatorial strategies to improve patient outcomes. We focused on those genetic events that augment response to venetoclax given the clinical need to develop venetoclax-based combinatorial treatment regimens for AML. Overall, our findings establish a functional link between splicing modulation and therapeutic efficacy of BCL2 inhibition in AML.

Given the established role of RNA splicing in regulating the expression and function of key proteins involved in cell death signaling and apoptosis, a number of prior studies have attempted to pharmacologically perturb splicing to promote response to BCL2 inhibition. For example, one prior study demonstrated that E7107, a potent SF3b inhibitor, can synergize with venetoclax in B cell malignancies and solid tumors.[58,59] However, toxicities associated with E7107 have led to its suspension from clinical use,[60,61] and the clinical efficacy of more recent SF3b inhibitors (such as the drug H3B-8800)[62] for high-risk myeloid neoplasms remains unclear. Here, we provide a rationale for a clinical modality to modulate RNA splicing through pharmacologic inhibition of splicing-dependent kinases. Specifically, our data suggest that inhibition of CLKs and DYRKs in combination with venetoclax or

(B) Dose-response curves of venetoclax-resistant MOLM-13 cells treated with different concentrations of venetoclax (top) and SM09419 (bottom) as indicated by x axis (n = 3; mean + SEM). Cell viability is denoted on the y axis.
(C) Schematic of patient-derived xenograft (PDX) generation and treated daily with SM09419 (25 mg/kg PO) or vehicle.
(D) Diagnosis, treatment regimen, and genetic characteristics of AML PDX samples.
(E and F) Percentage of human $CD45^+$ ($hCD45^+$) cells in (E) bone marrow and (F) peripheral blood of PDXs following 3 weeks of SM09419 treatment.
(G) Representative flow cytometry plots of $hCD45^+$ and mouse $CD45^+$ ($mCD45^+$) in bone marrow from PDXs treated daily with 25 mg/kg SM09419 after 3 weeks.
(H and I) Synergy scores (Loewe and HSA) (left) and 2D synergy plots (right) from *ex vivo*-cultured (H) patient 1 and (I) patient 2 samples treated with venetoclax, SM09419, or the combination after 48 h.

as a single agent represents a therapeutic strategy to circumvent resistance to venetoclax.

CLK and DYRK kinases are two highly related families of kinases within the CMGC (cyclin-dependent kinase [CDK], mitogen-activated protein kinase [MAPK], glycogen synthase kinase [GSK3], CLK) group of the eukaryotic kinome. Each CLK and DYRK is a dual-specificity kinase that phosphorylates serine/threonine and tyrosine residues.[63,64] A variety of structurally diverse CLK inhibitors have been developed, and most of these also inhibit DYRK kinases to varying degrees.[64] Despite the fact that CLKs and DYRKs perform multi-site phosphorylation of a number of substrates, it is clear that perturbing the activity of CLK1-4 or DYRK1A/B globally impacts RNA splicing via altering splicing factor protein phosphorylation. DYRK1A resides in nuclear speckles, and overexpression of DYRK1A induces redistribution of SR proteins from nuclear speckles to active sites of transcription/splicing in a manner that depends on its kinase activity.[65] Similarly, CLK1 has been shown to regulate the cellular localization and splicing impact of SRSF1 via phosphorylation of serine/proline dipeptides at multiple sites on SRSF1.[66]

Interestingly, prior data have identified that dephosphorylation of RNA splicing factors occurs during apoptosis, and that the ensuing change in splicing may be necessary for cells to execute apoptosis.[67] For example, SR proteins are targets for a number of apoptosis agonists, and splicing factor kinases are inactivated during cell death by caspase-mediated proteolysis.[67] This includes caspase-8, -9, and -3/6 cleaving SRPK1, SPRK2, and topoisomerase, respectively, thereby altering splicing during apoptosis. Moreover, FAS activation results in dephosphorylation of SR proteins via induction of PP1 phosphatase.[68] Thus, pharmacologic inhibition of phosphorylation of splicing factors may enhance response to venetoclax by mimicking the impact of apoptosis signaling cascade on RNA splicing.

SM09419 has pharmacologic properties that are very similar to Cirtuvivint, one of the first CLK/DYRK ATP-competitive inhibitors that has entered first-in-human and phase 1b clinical trials in patients with advanced solid tumors (ClinicalTrials.gov: NCT03355066 and NCT05084859).[69,70] In the Cirtuvivint first-in-human study, pharmacodynamic evidence for proof of mechanism in human whole blood was reported at well-tolerated doses. Importantly, infrequent grade 3 adverse hematologic events have been observed with a grade 3 anemia rate of <15% and even lower frequency for neutropenia or thrombocytopenia. In the dose-escalation portion of this trial and in the combination study, Cirtuvivint has shown early evidence of anti-tumor activity with declines in prostate-specific antigen (PSA) in prostate cancer subjects, tumor shrinkage in several tumor types, and prolonged stable disease (treatment reaching cycle 6 and beyond). Similarly, in the phase 1 trial of the pan-CLK inhibitor CTX-712 that evaluated subjects with solid tumors and hematologic malignancies, two complete remissions in refractory AML patients, along with two partial responses in ovarian cancers subjects, were reported with single-agent therapy.[71] Although it is too early to make conclusions about efficacy from these early data, hematologic recovery is required for CR in AML, which indicates that CLK/DYRK inhibition is feasible with manageable hematologic toxicity. Using the SM09419 compound herein, we provide preclinical data demonstrating the utility of CLK/DYRK inhibition as a single agent to overcome resistance to venetoclax-based therapies.

Beyond chemical modulation of RNA splicing, our genetic studies also highlighted a number of additional therapeutic targets to rationally enhance response to venetoclax and/or overcome venetoclax resistance. For instance, we demonstrated that loss of RBM10 enhances efficacy of venetoclax. RBM10 is a known splicing factor that promotes exon inclusion.[72] Although loss-of-function RBM10 mutations have been described in certain solid tumors[73–75] and in the genetic disease TARP (Talipes equinovarus, Atrial septal defect, Robin sequence, and Persistent left superior vena cava) syndrome,[76] we found that loss of Rbm10 does not alter hematopoiesis. These data suggest context-specific roles for RBM10 and nominate RBM10 as a therapeutic vulnerability in combination with BCL2 inhibitors.

Importantly, loss of RBM10 was associated with reduced expression of the anti-apoptotic BCL2 homolog *BCL2A1*, as well as alternative splicing of XIAP, the most well-characterized IAP protein. Among BCL2 family members, expression of *BCL2A1* has been most consistently associated with venetoclax resistance in a variety of leukemias. Upregulation of *BCL2A1* has been reported to be associated with resistance to venetoclax in both the BeatAML and Leucegene cohorts of AML patients, as well as AML preclinical models.[6,77] In addition, *BCL2A1* mRNA is heavily expressed (>10-fold more than BCL2) in monocytes, which is thought to at least partially explain the relationship between monocytic leukemia differentiation and impaired response to venetoclax.[6] Consistent with these findings, genetic downregulation of *BCL2A1* restores venetoclax sensitivity in AML models with venetoclax resistance.[6] Although there is no clinical means to chemically inhibit RBM10, our data underscore the need to develop potent small-molecule inhibitors or peptide aptamers of BCL2A1 in the treatment of AML.

Lastly, our data demonstrate that co-targeting of RBM10 and BCL2 or pharmacologic inhibition of CLK/DYRK converge on the mis-splicing of the IAP-antagonist protein, *XIAP*, as a mechanism to enhance venetoclax efficacy. These findings suggest the potential benefit of chemical campaigns to develop mimetics of IAP-antagonist proteins to negatively regulate *XIAP*, as seen with RBM10 loss.

LIMITATIONS OF THE STUDY

Here we describe the therapeutic rationale for the combination of venetoclax and SM09419, a multi-kinase inhibitor targeting CLK1–4, DYRK1A-B, and DYRK2 kinases. A limitation of this study is that it is currently unknown which of these specific kinase targets inhibited by SM09419 is responsible for exerting its function to sensitize AML cells to venetoclax therapy. This is a very important point given the development of other CLK and DYRK inhibitor agents that may be more selective for individual CLKs or DYRKs. Another limitation of this study is the evaluation of SM09419 across diverse genetic subtypes of AML. Given prior literature on the preferential sensitivity of splicing factor mutant myeloid leukemias via targeting of the spliceosome,[27,78,79] it will be important to test whether certain genetic alterations are more susceptible to SM09419.

STAR★METHODS

Detailed methods are provided in the online version of this paper and include the following:

- KEY RESOURCES TABLE
- RESOURCE AVAILABILITY
  - Lead contact
  - Material availability
  - Data and code availability
- EXPERIMENTAL MODEL AND SUBJECT DETAILS
  - Cell lines and cell culture
  - Animals
  - Human patient samples
- METHOD DETAILS
  - CRISPR screen
  - CRISPR indel analysis
  - RNA-sequencing library preparation and sequencing
  - eCLIP library preparation
  - Whole-exome sequencing and targeted capture sequencing
  - Western blotting
  - Colony-forming assays
  - Annexin V assay
  - Generation of Rbm10 conditional knockout mice
  - Bone marrow (BM) transplantation
  - Drug treatment IC_{50} measurements
  - QPCR measurement of BCL2A1 gene expression
  - cDNA overexpression
  - Animal experiments
  - Kinase assays
  - NanoBRET target engagement assay
  - Patient-derived xenograft experiments
- QUANTIFICATION AND STATISTICAL ANALYSIS
  - Genome-wide differential gene expression analysis
  - Gene expression estimation and alternative splicing analysis
  - Purine/Pyrimidine motif enrichment analysis
  - eCLIP data analysis
  - Gene ontology analysis
  - Statistical analysis

SUPPLEMENTAL INFORMATION

Supplemental information can be found online at https://doi.org/10.1016/j.ccell.2022.12.002.

ACKNOWLEDGMENTS

O.A.-W. and R.K.B. were supported by the Edward P. Evans Foundation, NIH/National Cancer Institute (NCI) (R01 CA251138), and NIH/National Heart, Lung, and Blood Institute (NHLBI) (R01 HL128239). O.A.-W. was supported by the NIH/NCI (R01 CA242020 and P50 CA254838-01) and The Leukemia & Lymphoma Society. R.K.B. was supported by the NIH/NHLBI (R01 HL151651) and the Blood Cancer Discoveries Grant program through the Leukemia & Lymphoma Society, Mark Foundation for Cancer Research, and Paul G. Allen Frontiers Group (8023-20). R.K.B. is a Scholar of The Leukemia & Lymphoma Society (1344-18) and holds the McIlwain Family Endowed Chair in Data Science. W.J.K. was supported by a Medical Scientist Training Program grant from the National Institute of General Medical Sciences of the NIH under award number T32GM007739 to the Weill Cornell/Rockefeller/Sloan Kettering Tri-Institutional MD-PhD Program. Computational studies were supported in part by FHCRC's Scientific Computing Infrastructure (ORIP S10 OD028685). We acknowledge the use of the Integrated Genomics Operation Core, supported by the NCI Cancer Center Support Grant (CCSG; P30 CA08748), Cycle for Survival, and the Marie-Josée and Henry R. Kravis Center for Molecular Oncology.

AUTHOR CONTRIBUTIONS

E.W., J.M.B.P., E.M., C.B., R.K.B., and O.A.-W. designed the study. E.W., E.C., C.B., and C.-C.M. performed *in vitro* experiments. E.W., J.B., W.J.K., S.C., M.E.S., D.C., C.E.E., K.K., R.F.S., S.M.T., and C.B. performed *in vivo* experiments. M.S. and J.P.B. identified and provided patient materials. J.M.B.P., S.J.H., E.M., and R.K.B. performed computational analyses. G.K., J.A.F., and O.A.-W. generated the Rbm10 cKO animal model. W.J.K., S.C., S.J.H., C.H., K.K., R.F.S., E.M., C.B., M.J., and D.M.B. assisted with experimental design and data interpretation. E.W., J.M.B.P., E.M., C.B., R.K.B., and O.A.-W. wrote the manuscript with input from all authors.

DECLARATION OF INTERESTS

E.M., E.C., M.J., C.B., C.-C.M., and D.M.B. are employees of Biosplice Therapeutics. O.A.-W. has served as a consultant for H3B Biomedicine, Foundation Medicine Inc., Merck, Prelude Therapeutics, and Janssen and is on the Scientific Advisory Board of Envisagenics Inc., AIChemy, Harmonic Discovery Inc., and Pfizer Boulder. O.A.-W. has received prior research funding from H3B Biomedicine, Nurix Therapeutics, and LOXO Oncology unrelated to the current manuscript. The remaining authors declare no competing interests.

Received: May 2, 2022
Revised: October 7, 2022
Accepted: December 5, 2022
Published: December 22, 2022

REFERENCES

1. Ferrara, F., and Schiffer, C.A. (2013). Acute myeloid leukaemia in adults. Lancet *381*, 484–495. https://doi.org/10.1016/S0140-6736(12)61727-9.
2. Short, N.J., Konopleva, M., Kadia, T.M., Borthakur, G., Ravandi, F., DiNardo, C.D., and Daver, N. (2020). Advances in the treatment of acute myeloid leukemia: new drugs and new challenges. Cancer Discov. *10*, 506–525. https://doi.org/10.1158/2159-8290.CD-19-1011.
3. Ganzel, C., Sun, Z., Cripe, L.D., Fernandez, H.F., Douer, D., Rowe, J.M., Paietta, E.M., Ketterling, R., O'Connell, M.J., Wiernik, P.H., et al. (2018). Very poor long-term survival in past and more recent studies for relapsed AML patients: the ECOG-ACRIN experience. Am. J. Hematol. *93*, 1074–1081. https://doi.org/10.1002/ajh.25162.
4. Breems, D.A., Van Putten, W.L.J., Huijgens, P.C., Ossenkoppele, G.J., Verhoef, G.E.G., Verdonck, L.F., Vellenga, E., De Greef, G.E., Jacky, E., Van der Lelie, J., et al. (2005). Prognostic index for adult patients with acute myeloid leukemia in first relapse. J. Clin. Oncol. *23*, 1969–1978. https://doi.org/10.1200/JCO.2005.06.027.
5. Nechiporuk, T., Kurtz, S.E., Nikolova, O., Liu, T., Jones, C.L., D'Alessandro, A., Culp-Hill, R., d'Almeida, A., Joshi, S.K., Rosenberg, M., et al. (2019). The TP53 apoptotic network is a primary mediator of resistance to BCL2 inhibition in AML cells. Cancer Discov. *9*, 910–925. https://doi.org/10.1158/2159-8290.CD-19-0125.
6. Zhang, H., Nakauchi, Y., Köhnke, T., Stafford, M., Bottomly, D., Thomas, R., Wilmot, B., McWeeney, S.K., Majeti, R., and Tyner, J.W. (2020). Integrated analysis of patient samples identifies biomarkers for venetoclax efficacy and combination strategies in acute myeloid leukemia. Nat. Cancer *1*, 826–839. https://doi.org/10.1038/s43018-020-0103-x.
7. Zuber, J., Radtke, I., Pardee, T.S., Zhao, Z., Rappaport, A.R., Luo, W., McCurrach, M.E., Yang, M.M., Dolan, M.E., Kogan, S.C., et al. (2009). Mouse models of human AML accurately predict chemotherapy response. Genes Dev. *23*, 877–889. https://doi.org/10.1101/gad.1771409.

8. Blombery, P., Lew, T.E., Dengler, M.A., Thompson, E.R., Lin, V.S., Chen, X., Nguyen, T., Panigrahi, A., Handunnetti, S.M., Carney, D.A., et al. (2022). Clonal hematopoiesis, myeloid disorders and BAX-mutated myelopoiesis in patients receiving venetoclax for CLL. Blood *139*, 1198–1207. https://doi.org/10.1182/blood.2021012775.

9. Kandoth, C., McLellan, M.D., Vandin, F., Ye, K., Niu, B., Lu, C., Xie, M., Zhang, Q., McMichael, J.F., Wyczalkowski, M.A., et al. (2013). Mutational landscape and significance across 12 major cancer types. Nature *502*, 333–339. https://doi.org/10.1038/nature12634.

10. Li, S., Garrett-Bakelman, F.E., Chung, S.S., Sanders, M.A., Hricik, T., Rapaport, F., Patel, J., Dillon, R., Vijay, P., Brown, A.L., et al. (2016). Distinct evolution and dynamics of epigenetic and genetic heterogeneity in acute myeloid leukemia. Nat. Med. *22*, 792–799. https://doi.org/10.1038/nm.4125.

11. Fennell, K.A., Vassiliadis, D., Lam, E.Y.N., Martelotto, L.G., Balic, J.J., Hollizeck, S., Weber, T.S., Semple, T., Wang, Q., Miles, D.C., et al. (2022). Non-genetic determinants of malignant clonal fitness at single-cell resolution. Nature *601*, 125–131. https://doi.org/10.1038/s41586-021-04206-7.

12. Konopleva, M., Pollyea, D.A., Potluri, J., Chyla, B., Hogdal, L., Busman, T., McKeegan, E., Salem, A.H., Zhu, M., Ricker, J.L., et al. (2016). Efficacy and biological correlates of response in a phase II study of venetoclax monotherapy in patients with acute myelogenous leukemia. Cancer Discov. *6*, 1106–1117. https://doi.org/10.1158/2159-8290.CD-16-0313.

13. Minn, A.J., Rudin, C.M., Boise, L.H., and Thompson, C.B. (1995). Expression of bcl-xL can confer a multidrug resistance phenotype. Blood *86*, 1903–1910.

14. Jones, C.L., Stevens, B.M., Pollyea, D.A., Culp-Hill, R., Reisz, J.A., Nemkov, T., Gehrke, S., Gamboni, F., Krug, A., Winters, A., et al. (2020). Nicotinamide metabolism mediates resistance to venetoclax in relapsed acute myeloid leukemia stem cells. Cell Stem Cell *27*, 748–764.e4. https://doi.org/10.1016/j.stem.2020.07.021.

15. Jones, C.L., Stevens, B.M., D'Alessandro, A., Reisz, J.A., Culp-Hill, R., Nemkov, T., Pei, S., Khan, N., Adane, B., Ye, H., et al. (2018). Inhibition of amino acid metabolism selectively targets human leukemia stem cells. Cancer Cell *34*, 724–740.e4. https://doi.org/10.1016/j.ccell.2018.10.005.

16. Chen, X., Glytsou, C., Zhou, H., Narang, S., Reyna, D.E., Lopez, A., Sakellaropoulos, T., Gong, Y., Kloetgen, A., Yap, Y.S., et al. (2019). Targeting mitochondrial structure sensitizes acute myeloid leukemia to venetoclax treatment. Cancer Discov. *9*, 890–909. https://doi.org/10.1158/2159-8290.CD-19-0117.

17. Fong, C.Y., Gilan, O., Lam, E.Y.N., Rubin, A.F., Ftouni, S., Tyler, D., Stanley, K., Sinha, D., Yeh, P., Morison, J., et al. (2015). BET inhibitor resistance emerges from leukaemia stem cells. Nature *525*, 538–542. https://doi.org/10.1038/nature14888.

18. Rathert, P., Roth, M., Neumann, T., Muerdter, F., Roe, J.S., Muhar, M., Deswal, S., Cerny-Reiterer, S., Peter, B., Jude, J., et al. (2015). Transcriptional plasticity promotes primary and acquired resistance to BET inhibition. Nature *525*, 543–547. https://doi.org/10.1038/nature14898.

19. Rini, B.I., Plimack, E.R., Stus, V., Gafanov, R., Hawkins, R., Nosov, D., Pouliot, F., Alekseev, B., Soulières, D., Melichar, B., et al. (2019). Pembrolizumab plus axitinib versus sunitinib for advanced renal-cell carcinoma. N. Engl. J. Med. *380*, 1116–1127. https://doi.org/10.1056/NEJMoa1816714.

20. Baselga, J., Cortés, J., Kim, S.B., Im, S.A., Hegg, R., Im, Y.H., Roman, L., Pedrini, J.L., Pienkowski, T., Knott, A., et al. (2012). Pertuzumab plus trastuzumab plus docetaxel for metastatic breast cancer. N. Engl. J. Med. *366*, 109–119. https://doi.org/10.1056/NEJMoa1113216.

21. DiNardo, C.D., Pratz, K.W., Letai, A., Jonas, B.A., Wei, A.H., Thirman, M., Arellano, M., Frattini, M.G., Kantarjian, H., Popovic, R., et al. (2018). Safety and preliminary efficacy of venetoclax with decitabine or azacitidine in elderly patients with previously untreated acute myeloid leukaemia: a non-randomised, open-label, phase 1b study. Lancet Oncol. *19*, 216–228. https://doi.org/10.1016/S1470-2045(18)30010-X.

22. DiNardo, C.D., Jonas, B.A., Pullarkat, V., Thirman, M.J., Garcia, J.S., Wei, A.H., Konopleva, M., Döhner, H., Letai, A., Fenaux, P., et al. (2020). Azacitidine and venetoclax in previously untreated acute myeloid leukemia. N. Engl. J. Med. *383*, 617–629. https://doi.org/10.1056/NEJMoa2012971.

23. Schwerk, C., and Schulze-Osthoff, K. (2005). Regulation of apoptosis by alternative pre-mRNA splicing. Mol. Cell *19*, 1–13. https://doi.org/10.1016/j.molcel.2005.05.026.

24. Sanson, K.R., Hanna, R.E., Hegde, M., Donovan, K.F., Strand, C., Sullender, M.E., Vaimberg, E.W., Goodale, A., Root, D.E., Piccioni, F., and Doench, J.G. (2018). Optimized libraries for CRISPR-Cas9 genetic screens with multiple modalities. Nat. Commun. *9*, 5416. https://doi.org/10.1038/s41467-018-07901-8.

25. Gu, X., Tohme, R., Tomlinson, B., Sakre, N., Hasipek, M., Durkin, L., Schuerger, C., Grabowski, D., Zidan, A.M., Radivoyevitch, T., et al. (2021). Decitabine- and 5-azacytidine resistance emerges from adaptive responses of the pyrimidine metabolism network. Leukemia *35*, 1023–1036. https://doi.org/10.1038/s41375-020-1003-x.

26. Sripayap, P., Nagai, T., Uesawa, M., Kobayashi, H., Tsukahara, T., Ohmine, K., Muroi, K., and Ozawa, K. (2014). Mechanisms of resistance to azacitidine in human leukemia cell lines. Exp. Hematol. *42*, 294–306.e2. https://doi.org/10.1016/j.exphem.2013.12.004.

27. Wang, E., Lu, S.X., Pastore, A., Chen, X., Imig, J., Chun-Wei Lee, S., Hockemeyer, K., Ghebrechristos, Y.E., Yoshimi, A., Inoue, D., et al. (2019). Targeting an RNA-binding protein network in acute myeloid leukemia. Cancer Cell *35*, 369–384.e7. https://doi.org/10.1016/j.ccell.2019.01.010.

28. Zhou, Y., Han, C., Wang, E., Lorch, A.H., Serafin, V., Cho, B.K., Gutierrez Diaz, B.T., Calvo, J., Fang, C., Khodadadi-Jamayran, A., et al. (2020). Posttranslational regulation of the exon skipping machinery controls aberrant splicing in leukemia. Cancer Discov. *10*, 1388–1409. https://doi.org/10.1158/2159-8290.CD-19-1436.

29. Wang, E., Zhou, H., Nadorp, B., Cayanan, G., Chen, X., Yeaton, A.H., Nomikou, S., Witkowski, M.T., Narang, S., Kloetgen, A., et al. (2021). Surface antigen-guided CRISPR screens identify regulators of myeloid leukemia differentiation. Cell Stem Cell *28*, 718–731.e6. https://doi.org/10.1016/j.stem.2020.12.005.

30. Witkowski, M.T., Lee, S., Wang, E., Lee, A.K., Talbot, A., Ma, C., Tsopoulidis, N., Brumbaugh, J., Zhao, Y., Roberts, K.G., et al. (2022). NUDT21 limits CD19 levels through alternative mRNA polyadenylation in B cell acute lymphoblastic leukemia. Nat. Immunol. *23*, 1424–1432. https://doi.org/10.1038/s41590-022-01314-y.

31. Han, C., Khodadadi-Jamayran, A., Lorch, A.H., Jin, Q., Serafin, V., Zhu, P., Politanska, Y., Sun, L., Gutierrez-Diaz, B.T., Pryzhkova, M.V., et al. (2022). SF3B1 homeostasis is critical for survival and therapeutic response in T cell leukemia. Sci. Adv. *8*, eabj8357. https://doi.org/10.1126/sciadv.abj8357.

32. Lachowiez, C.A., Loghavi, S., Furudate, K., Montalban-Bravo, G., Maiti, A., Kadia, T., Daver, N., Borthakur, G., Pemmaraju, N., Sasaki, K., et al. (2021). Impact of splicing mutations in acute myeloid leukemia treated with hypomethylating agents combined with venetoclax. Blood Adv. *5*, 2173–2183. https://doi.org/10.1182/bloodadvances.2020004173.

33. Shi, J., Wang, E., Milazzo, J.P., Wang, Z., Kinney, J.B., and Vakoc, C.R. (2015). Discovery of cancer drug targets by CRISPR-Cas9 screening of protein domains. Nat. Biotechnol. *33*, 661–667. https://doi.org/10.1038/nbt.3235.

34. Sugimoto, K., Toyoshima, H., Sakai, R., Miyagawa, K., Hagiwara, K., Ishikawa, F., Takaku, F., Yazaki, Y., and Hirai, H. (1992). Frequent mutations in the p53 gene in human myeloid leukemia cell lines. Blood *79*, 2378–2383.

35. Hart, T., Chandrashekhar, M., Aregger, M., Steinhart, Z., Brown, K.R., MacLeod, G., Mis, M., Zimmermann, M., Fradet-Turcotte, A., Sun, S., et al. (2015). High-Resolution CRISPR screens reveal fitness genes and genotype-specific cancer liabilities. Cell *163*, 1515–1526. https://doi.org/10.1016/j.cell.2015.11.015.

36. Collins, K.M., Kainov, Y.A., Christodolou, E., Ray, D., Morris, Q., Hughes, T., Taylor, I.A., Makeyev, E.V., and Ramos, A. (2017). An RRM-ZnF RNA recognition module targets RBM10 to exonic sequences to promote exon exclusion. Nucleic Acids Res. *45*, 6761–6774. https://doi.org/10.1093/nar/gkx225.

37. Van Nostrand, E.L., Pratt, G.A., Shishkin, A.A., Gelboin-Burkhart, C., Fang, M.Y., Sundararaman, B., Blue, S.M., Nguyen, T.B., Surka, C., Elkins, K., et al. (2016). Robust transcriptome-wide discovery of RNA-binding protein binding sites with enhanced CLIP (eCLIP). Nat. Methods *13*, 508–514. https://doi.org/10.1038/nmeth.3810.

38. Shiozaki, E.N., Chai, J., Rigotti, D.J., Riedl, S.J., Li, P., Srinivasula, S.M., Alnemri, E.S., Fairman, R., and Shi, Y. (2003). Mechanism of XIAP-mediated inhibition of caspase-9. Mol. Cell *11*, 519–527. https://doi.org/10.1016/s1097-2765(03)00054-6.

39. Srinivasula, S.M., Hegde, R., Saleh, A., Datta, P., Shiozaki, E., Chai, J., Lee, R.A., Robbins, P.D., Fernandes-Alnemri, T., Shi, Y., and Alnemri, E.S. (2001). A conserved XIAP-interaction motif in caspase-9 and Smac/DIABLO regulates caspase activity and apoptosis. Nature *410*, 112–116. https://doi.org/10.1038/35065125.

40. Huang, Y., Park, Y.C., Rich, R.L., Segal, D., Myszka, D.G., and Wu, H. (2001). Structural basis of caspase inhibition by XIAP: differential roles of the linker versus the BIR domain. Cell *104*, 781–790.

41. Riedl, S.J., Renatus, M., Schwarzenbacher, R., Zhou, Q., Sun, C., Fesik, S.W., Liddington, R.C., and Salvesen, G.S. (2001). Structural basis for the inhibition of caspase-3 by XIAP. Cell *104*, 791–800. https://doi.org/10.1016/s0092-8674(01)00274-4.

42. Hashimoto, M., Saito, Y., Nakagawa, R., Ogahara, I., Takagi, S., Takata, S., Amitani, H., Endo, M., Yuki, H., Ramilowski, J.A., et al. (2021). Combined inhibition of XIAP and BCL2 drives maximal therapeutic efficacy in genetically diverse aggressive acute myeloid leukemia. Nat. Cancer *2*, 340–356. https://doi.org/10.1038/s43018-021-00177-w.

43. Tyner, J.W., Tognon, C.E., Bottomly, D., Wilmot, B., Kurtz, S.E., Savage, S.L., Long, N., Schultz, A.R., Traer, E., Abel, M., et al. (2018). Functional genomic landscape of acute myeloid leukaemia. Nature *562*, 526–531. https://doi.org/10.1038/s41586-018-0623-z.

44. Gui, J.F., Tronchère, H., Chandler, S.D., and Fu, X.D. (1994). Purification and characterization of a kinase specific for the serine- and arginine-rich pre-mRNA splicing factors. Proc. Natl. Acad. Sci. USA *91*, 10824–10828. https://doi.org/10.1073/pnas.91.23.10824.

45. Aubol, B.E., Wu, G., Keshwani, M.M., Movassat, M., Fattet, L., Hertel, K.J., Fu, X.D., and Adams, J.A. (2016). Release of SR proteins from CLK1 by SRPK1: a symbiotic kinase system for phosphorylation control of pre-mRNA splicing. Mol. Cell *63*, 218–228. https://doi.org/10.1016/j.molcel.2016.05.034.

46. Colwill, K., Feng, L.L., Yeakley, J.M., Gish, G.D., Cáceres, J.F., Pawson, T., and Fu, X.D. (1996). SRPK1 and Clk/Sty protein kinases show distinct substrate specificities for serine/arginine-rich splicing factors. J. Biol. Chem. *271*, 24569–24575. https://doi.org/10.1074/jbc.271.40.24569.

47. Prasad, J., Colwill, K., Pawson, T., and Manley, J.L. (1999). The protein kinase Clk/Sty directly modulates SR protein activity: both hyper- and hypophosphorylation inhibit splicing. Mol. Cell Biol. *19*, 6991–7000. https://doi.org/10.1128/MCB.19.10.6991.

48. Qian, W., Liang, H., Shi, J., Jin, N., Grundke-Iqbal, I., Iqbal, K., Gong, C.X., and Liu, F. (2011). Regulation of the alternative splicing of tau exon 10 by SC35 and Dyrk1A. Nucleic Acids Res. *39*, 6161–6171. https://doi.org/10.1093/nar/gkr195.

49. Shi, J., Zhang, T., Zhou, C., Chohan, M.O., Gu, X., Wegiel, J., Zhou, J., Hwang, Y.W., Iqbal, K., Grundke-Iqbal, I., et al. (2008). Increased dosage of Dyrk1A alters alternative splicing factor (ASF)-regulated alternative splicing of tau in Down syndrome. J. Biol. Chem. *283*, 28660–28669. https://doi.org/10.1074/jbc.M802645200.

50. de Graaf, K., Czajkowska, H., Rottmann, S., Packman, L.C., Lilischkis, R., Lüscher, B., and Becker, W. (2006). The protein kinase DYRK1A phosphorylates the splicing factor SF3b1/SAP155 at Thr434, a novel in vivo phosphorylation site. BMC Biochem. *7*, 7. https://doi.org/10.1186/1471-2091-7-7.

51. Meyers, R.M., Bryan, J.G., McFarland, J.M., Weir, B.A., Sizemore, A.E., Xu, H., Dharia, N.V., Montgomery, P.G., Cowley, G.S., Pantel, S., et al. (2017). Computational correction of copy number effect improves specificity of CRISPR-Cas9 essentiality screens in cancer cells. Nat. Genet. *49*, 1779–1784. https://doi.org/10.1038/ng.3984.

52. Düwel, M., Welteke, V., Oeckinghaus, A., Baens, M., Kloo, B., Ferch, U., Darnay, B.G., Ruland, J., Marynen, P., and Krappmann, D. (2009). A20 negatively regulates T cell receptor signaling to NF-kappaB by cleaving Malt1 ubiquitin chains. J. Immunol. *182*, 7718–7728. https://doi.org/10.4049/jimmunol.0803313.

53. Zuber, J., Rappaport, A.R., Luo, W., Wang, E., Chen, C., Vaseva, A.V., Shi, J., Weissmueller, S., Fellmann, C., Taylor, M.J., et al. (2011). An integrated approach to dissecting oncogene addiction implicates a Myb-coordinated self-renewal program as essential for leukemia maintenance. Genes Dev. *25*, 1628–1640. https://doi.org/10.1101/gad.17269211.

54. Zuber, J., Shi, J., Wang, E., Rappaport, A.R., Herrmann, H., Sison, E.A., Magoon, D., Qi, J., Blatt, K., Wunderlich, M., et al. (2011). RNAi screen identifies Brd4 as a therapeutic target in acute myeloid leukaemia. Nature *478*, 524–528. https://doi.org/10.1038/nature10334.

55. Sykes, D.B., Kfoury, Y.S., Mercier, F.E., Wawer, M.J., Law, J.M., Haynes, M.K., Lewis, T.A., Schajnovitz, A., Jain, E., Lee, D., et al. (2016). Inhibition of dihydroorotate dehydrogenase overcomes differentiation blockade in acute myeloid leukemia. Cell *167*, 171–186.e15. https://doi.org/10.1016/j.cell.2016.08.057.

56. Kim, J., Woo, A.J., Chu, J., Snow, J.W., Fujiwara, Y., Kim, C.G., Cantor, A.B., and Orkin, S.H. (2010). A Myc network accounts for similarities between embryonic stem and cancer cell transcription programs. Cell *143*, 313–324. https://doi.org/10.1016/j.cell.2010.09.010.

57. Somervaille, T.C.P., Matheny, C.J., Spencer, G.J., Iwasaki, M., Rinn, J.L., Witten, D.M., Chang, H.Y., Shurtleff, S.A., Downing, J.R., and Cleary, M.L. (2009). Hierarchical maintenance of MLL myeloid leukemia stem cells employs a transcriptional program shared with embryonic rather than adult stem cells. Cell Stem Cell *4*, 129–140. https://doi.org/10.1016/j.stem.2008.11.015.

58. Aird, D., Teng, T., Huang, C.L., Pazolli, E., Banka, D., Cheung-Ong, K., Eifert, C., Furman, C., Wu, Z.J., Seiler, M., et al. (2019). Sensitivity to splicing modulation of BCL2 family genes defines cancer therapeutic strategies for splicing modulators. Nat. Commun. *10*, 137. https://doi.org/10.1038/s41467-018-08150-5.

59. Ten Hacken, E., Valentin, R., Regis, F.F.D., Sun, J., Yin, S., Werner, L., Deng, J., Gruber, M., Wong, J., Zheng, M., et al. (2018). Splicing modulation sensitizes chronic lymphocytic leukemia cells to venetoclax by remodeling mitochondrial apoptotic dependencies. JCI Insight *3*, e121438. https://doi.org/10.1172/jci.insight.121438.

60. Hong, D.S., Kurzrock, R., Naing, A., Wheler, J.J., Falchook, G.S., Schiffman, J.S., Faulkner, N., Pilat, M.J., O'Brien, J., and LoRusso, P. (2014). A phase I, open-label, single-arm, dose-escalation study of E7107, a precursor messenger ribonucleic acid (pre-mRNA) splicesome inhibitor administered intravenously on days 1 and 8 every 21 days to patients with solid tumors. Invest. N. Drugs *32*, 436–444. https://doi.org/10.1007/s10637-013-0046-5.

61. Eskens, F.A.L.M., Ramos, F.J., Burger, H., O'Brien, J.P., Piera, A., de Jonge, M.J.A., Mizui, Y., Wiemer, E.A.C., Carreras, M.J., Baselga, J., and Tabernero, J. (2013). Phase I pharmacokinetic and pharmacodynamic study of the first-in-class spliceosome inhibitor E7107 in patients with advanced solid tumors. Clin. Cancer Res. *19*, 6296–6304. https://doi.org/10.1158/1078-0432.CCR-13-0485.

62. Seiler, M., Yoshimi, A., Darman, R., Chan, B., Keaney, G., Thomas, M., Agrawal, A.A., Caleb, B., Csibi, A., Sean, E., et al. (2018). H3B-8800, an orally available small-molecule splicing modulator, induces lethality in spliceosome-mutant cancers. Nat. Med. *24*, 497–504. https://doi.org/10.1038/nm.4493.

63. Lindberg, M.F., and Meijer, L. (2021). Dual-specificity, tyrosine phosphorylation-regulated kinases (DYRKs) and cdc2-like kinases (CLKs) in human disease, an overview. Int. J. Mol. Sci. *22*, 6047. https://doi.org/10.3390/ijms22116047.

64. Martín Moyano, P., Němec, V., and Paruch, K. (2020). Cdc-like kinases (CLKs): biology, chemical probes, and therapeutic potential. Int. J. Mol. Sci. *21*, 7549. https://doi.org/10.3390/ijms21207549.

65. Alvarez, M., Estivill, X., and de la Luna, S. (2003). DYRK1A accumulates in splicing speckles through a novel targeting signal and induces speckle disassembly. J. Cell Sci. *116*, 3099–3107. https://doi.org/10.1242/jcs.00618.

66. Aubol, B.E., Plocinik, R.M., Hagopian, J.C., Ma, C.T., McGlone, M.L., Bandyopadhyay, R., Fu, X.D., and Adams, J.A. (2013). Partitioning RS domain phosphorylation in an SR protein through the CLK and SRPK protein kinases. J. Mol. Biol. *425*, 2894–2909. https://doi.org/10.1016/j.jmb.2013.05.013.

67. Kamachi, M., Le, T.M., Kim, S.J., Geiger, M.E., Anderson, P., and Utz, P.J. (2002). Human autoimmune sera as molecular probes for the identification of an autoantigen kinase signaling pathway. J. Exp. Med. *196*, 1213–1225. https://doi.org/10.1084/jem.20021167.

68. Chalfant, C.E., Ogretmen, B., Galadari, S., Kroesen, B.J., Pettus, B.J., and Hannun, Y.A. (2001). FAS activation induces dephosphorylation of SR proteins; dependence on the de novo generation of ceramide and activation of protein phosphatase 1. J. Biol. Chem. *276*, 44848–44855. https://doi.org/10.1074/jbc.M106291200.

69. Tolcher, A., Babiker, H.M., Chung, V., Kim, E., Moser, J., Karim, R., Vandross, A., Sommerhalder, D., Scott, A.J., Fakih, M., et al. (2021). Abstract CT112: initial results from a Phase 1 trial of a first-in-class pan-CDC-like kinase inhibitor (SM08502) with proof of mechanism in subjects with advanced solid tumors. Cancer Res. *81*, CT112. https://doi.org/10.1158/1538-7445.Am2021-ct112.

70. Scott, A., Call, J.A., Chandana, S., Borazanci, E., Falchook, G.S., Bordoni, R., Richey, S., Starodub, A., Chung, V., Lakhani, N.J., et al. (2022). 451O Preliminary evidence of clinical activity from phase I and Ib trials of the CLK/DYRK inhibitor cirtuvivint (CIRT) in subjects with advanced solid tumors. Ann. Oncol. *33*, S742–S743. https://doi.org/10.1016/j.annonc.2022.07.580.

71. Shimizu, T., Yonemori, K., Koyama, T., Katsuya, Y., Sato, J., Fukuhara, N., Yokoyama, H., Iida, H., Ando, K., Fukuhara, S., et al. (2022). A first-in-human phase I study of CTX-712 in patients with advanced, relapsed or refractory malignant tumors. J. Clin. Oncol. *40*, 3080. https://doi.org/10.1200/JCO.2022.40.16_suppl.3080.

72. Wang, Y., Gogol-Döring, A., Hu, H., Fröhler, S., Ma, Y., Jens, M., Maaskola, J., Murakawa, Y., Quedenau, C., Landthaler, M., et al. (2013). Integrative analysis revealed the molecular mechanism underlying RBM10-mediated splicing regulation. EMBO Mol. Med. *5*, 1431–1442. https://doi.org/10.1002/emmm.201302663.

73. Witkiewicz, A.K., McMillan, E.A., Balaji, U., Baek, G., Lin, W.C., Mansour, J., Mollaee, M., Wagner, K.U., Koduru, P., Yopp, A., et al. (2015). Whole-exome sequencing of pancreatic cancer defines genetic diversity and therapeutic targets. Nat. Commun. *6*, 6744. https://doi.org/10.1038/ncomms7744.

74. Cancer Genome Atlas Research Network (2014). Comprehensive molecular profiling of lung adenocarcinoma. Nature *511*, 543–550. https://doi.org/10.1038/nature13385.

75. Giannakis, M., Mu, X.J., Shukla, S.A., Qian, Z.R., Cohen, O., Nishihara, R., Bahl, S., Cao, Y., Amin-Mansour, A., Yamauchi, M., et al. (2016). Genomic correlates of immune-cell infiltrates in colorectal carcinoma. Cell Rep. *15*, 857–865. https://doi.org/10.1016/j.celrep.2016.03.075.

76. Gripp, K.W., Hopkins, E., Johnston, J.J., Krause, C., Dobyns, W.B., and Biesecker, L.G. (2011). Long-term survival in TARP syndrome and confirmation of RBM10 as the disease-causing gene. Am. J. Med. Genet. *155A*, 2516–2520. https://doi.org/10.1002/ajmg.a.34190.

77. Bisaillon, R., Moison, C., Thiollier, C., Krosl, J., Bordeleau, M.E., Lehnertz, B., Lavallée, V.P., MacRae, T., Mayotte, N., Labelle, C., et al. (2020). Genetic characterization of ABT-199 sensitivity in human AML. Leukemia *34*, 63–74. https://doi.org/10.1038/s41375-019-0485-x.

78. Obeng, E.A., Chappell, R.J., Seiler, M., Chen, M.C., Campagna, D.R., Schmidt, P.J., Schneider, R.K., Lord, A.M., Wang, L., Gambe, R.G., et al. (2016). Physiologic expression of Sf3b1(K700E) causes impaired erythropoiesis, aberrant splicing, and sensitivity to therapeutic spliceosome modulation. Cancer Cell *30*, 404–417. https://doi.org/10.1016/j.ccell.2016.08.006.

79. Lee, S.C.W., and Abdel-Wahab, O. (2016). Therapeutic targeting of splicing in cancer. Nat. Med. *22*, 976–986. https://doi.org/10.1038/nm.4165.

80. Sanjana, N.E., Shalem, O., and Zhang, F. (2014). Improved vectors and genome-wide libraries for CRISPR screening. Nat. Methods *11*, 783–784. https://doi.org/10.1038/nmeth.3047.

81. Cheng, D.T., Mitchell, T.N., Zehir, A., Shah, R.H., Benayed, R., Syed, A., Chandramohan, R., Liu, Z.Y., Won, H.H., Scott, S.N., et al. (2015). Memorial sloan kettering-integrated mutation profiling of actionable cancer targets (MSK-IMPACT): a hybridization capture-based next-generation sequencing clinical assay for solid tumor molecular Oncology. J. Mol. Diagn. *17*, 251–264. https://doi.org/10.1016/j.jmoldx.2014.12.006.

82. Zehir, A., Benayed, R., Shah, R.H., Syed, A., Middha, S., Kim, H.R., Srinivasan, P., Gao, J., Chakravarty, D., Devlin, S.M., et al. (2017). Mutational landscape of metastatic cancer revealed from prospective clinical sequencing of 10, 000 patients. Nat. Med. *23*, 703–713. https://doi.org/10.1038/nm.4333.

83. Doench, J.G., Fusi, N., Sullender, M., Hegde, M., Vaimberg, E.W., Donovan, K.F., Smith, I., Tothova, Z., Wilen, C., Orchard, R., et al. (2016). Optimized sgRNA design to maximize activity and minimize off-target effects of CRISPR-Cas9. Nat. Biotechnol. *34*, 184–191. https://doi.org/10.1038/nbt.3437.

84. Tarumoto, Y., Lu, B., Somerville, T.D.D., Huang, Y.H., Milazzo, J.P., Wu, X.S., Klingbeil, O., El Demerdash, O., Shi, J., and Vakoc, C.R. (2018). LKB1, salt-inducible kinases, and MEF2C are linked dependencies in acute myeloid leukemia. Mol. Cell *69*, 1017–1027.e6. https://doi.org/10.1016/j.molcel.2018.02.011.

85. Pinello, L., Canver, M.C., Hoban, M.D., Orkin, S.H., Kohn, D.B., Bauer, D.E., and Yuan, G.C. (2016). Analyzing CRISPR genome-editing experiments with CRISPResso. Nat. Biotechnol. *34*, 695–697. https://doi.org/10.1038/nbt.3583.

86. Demidenko, E., and Miller, T.W. (2019). Statistical determination of synergy based on Bliss definition of drugs independence. PLoS One *14*, e0224137. https://doi.org/10.1371/journal.pone.0224137.

87. Metz, K.S., Deoudes, E.M., Berginski, M.E., Jimenez-Ruiz, I., Aksoy, B.A., Hammerbacher, J., Gomez, S.M., and Phanstiel, D.H. (2018). Coral: clear and customizable visualization of human kinome data. Cell Syst. *7*, 347–350.e1. https://doi.org/10.1016/j.cels.2018.07.001.

88. Martin, M. (2011). Cutadapt removes adapter sequences from high-throughput sequencing reads. EMBnet. J. *17*, 3. https://doi.org/10.14806/ej.17.1.200.

89. Dobin, A., Davis, C.A., Schlesinger, F., Drenkow, J., Zaleski, C., Jha, S., Batut, P., Chaisson, M., and Gingeras, T.R. (2013). STAR: ultrafast universal RNA-seq aligner. Bioinformatics *29*, 15–21. https://doi.org/10.1093/bioinformatics/bts635.

90. Danecek, P., Bonfield, J.K., Liddle, J., Marshall, J., Ohan, V., Pollard, M.O., Whitwham, A., Keane, T., McCarthy, S.A., Davies, R.M., and Li, H. (2021). Twelve years of SAMtools and BCFtools. GigaScience *10*, giab008. https://doi.org/10.1093/gigascience/giab008.

91. Ramírez, F., Ryan, D.P., Grüning, B., Bhardwaj, V., Kilpert, F., Richter, A.S., Heyne, S., Dündar, F., and Manke, T. (2016). deepTools2: a next generation web server for deep-sequencing data analysis. Nucleic Acids Res. *44*, W160–W165. https://doi.org/10.1093/nar/gkw257.

92. Liao, Y., Smyth, G.K., and Shi, W. (2014). featureCounts: an efficient general purpose program for assigning sequence reads to genomic features. Bioinformatics *30*, 923–930.

93. Meyer, L.R., Zweig, A.S., Hinrichs, A.S., Karolchik, D., Kuhn, R.M., Wong, M., Sloan, C.A., Rosenbloom, K.R., Roe, G., Rhead, B., et al. (2013). The UCSC Genome Browser database: extensions and updates 2013. Nucleic Acids Res. *41*, D64–D69. https://doi.org/10.1093/nar/gks1048.

94. Flicek, P., Ahmed, I., Amode, M.R., Barrell, D., Beal, K., Brent, S., Carvalho-Silva, D., Clapham, P., Coates, G., Fairley, S., et al. (2013). Ensembl 2013. Nucleic Acids Res. *41*, D48–D55. https://doi.org/10.1093/nar/gks1236.

95. Katz, Y., Wang, E.T., Airoldi, E.M., and Burge, C.B. (2010). Analysis and design of RNA sequencing experiments for identifying isoform regulation. Nat. Methods *7*, 1009–1015. https://doi.org/10.1038/nmeth.1528.

96. Li, B., and Dewey, C.N. (2011). RSEM: accurate transcript quantification from RNA-Seq data with or without a reference genome. BMC Bioinf. *12*, 323. https://doi.org/10.1186/1471-2105-12-323.

97. Langmead, B., Trapnell, C., Pop, M., and Salzberg, S.L. (2009). Ultrafast and memory-efficient alignment of short DNA sequences to the human genome. Genome Biol. *10*, R25. https://doi.org/10.1186/gb-2009-10-3-r25.

98. Robinson, M.D., and Oshlack, A. (2010). A scaling normalization method for differential expression analysis of RNA-seq data. Genome Biol. *11*, R25. https://doi.org/10.1186/gb-2010-11-3-r25.

99. Trapnell, C., Pachter, L., and Salzberg, S.L. (2009). TopHat: discovering splice junctions with RNA-Seq. Bioinformatics *25*, 1105–1111. https://doi.org/10.1093/bioinformatics/btp120.

100. Huber, W., Carey, V.J., Gentleman, R., Anders, S., Carlson, M., Carvalho, B.S., Bravo, H.C., Davis, S., Gatto, L., Girke, T., et al. (2015). Orchestrating high-throughput genomic analysis with Bioconductor. Nat. Methods *12*, 115–121. https://doi.org/10.1038/nmeth.3252.

101. Wickham, H., Averick, M., Bryan, J., Chang, W., McGowan, L., François, R., Grolemund, G., Hayes, A., Henry, L., Hester, J., et al. (2019). Welcome to the tidyverse. Journal of open source software *4*, 1686.

102. Conway, J.R., Lex, A., and Gehlenborg, N. (2017). UpSetR: an R package for the visualization of intersecting sets and their properties. Bioinformatics *33*, 2938–2940. https://doi.org/10.1093/bioinformatics/btx364.

103. Breese, M.R., and Liu, Y. (2013). NGSUtils: a software suite for analyzing and manipulating next-generation sequencing datasets. Bioinformatics *29*, 494–496. https://doi.org/10.1093/bioinformatics/bts731.

104. Anders, S., Pyl, P.T., and Huber, W. (2015). HTSeq–a Python framework to work with high-throughput sequencing data. Bioinformatics *31*, 166–169. https://doi.org/10.1093/bioinformatics/btu638.

105. Huppertz, I., Perez-Perri, J.I., Mantas, P., Sekaran, T., Schwarzl, T., Russo, F., Ferring-Appel, D., Koskova, Z., Dimitrova-Paternoga, L., Kafkia, E., et al. (2022). Riboregulation of Enolase 1 activity controls glycolysis and embryonic stem cell differentiation. Mol. Cell *82*, 2666–2680.e11. https://doi.org/10.1016/j.molcel.2022.05.019.

106. Lawrence, M., Huber, W., Pagès, H., Aboyoun, P., Carlson, M., Gentleman, R., Morgan, M.T., and Carey, V.J. (2013). Software for computing and annotating genomic ranges. PLoS Comput. Biol. *9*, e1003118. https://doi.org/10.1371/journal.pcbi.1003118.

107. Ignatiadis, N., Klaus, B., Zaugg, J.B., and Huber, W. (2016). Data-driven hypothesis weighting increases detection power in genome-scale multiple testing. Nat. Methods *13*, 577–580. https://doi.org/10.1038/nmeth.3885.

108. Korotkevich, G., Sukhov, V., Budin, N., Shpak, B., Artyomov, M.N., and Sergushichev, A. (2021). Fast gene set enrichment analysis. Preprint at bioRxiv060012. https://doi.org/10.1101/060012.

STAR★METHODS

KEY RESOURCES TABLE

REAGENT or RESOURCE	SOURCE	IDENTIFIER
Antibodies		
TruStain Fcblock	BioLegends	422302; RRID: AB_2818986
Anti-RBM10 rabbit polyclonal	Bethyl Laboratories	A301-006A; RRID: AB_2175726
B-actin HRP	Sigma Aldrich	A3854; RRID: AB_262011
Anti-Phosphoepitope SR proteins Antibody, clone 1H4	Millipore Sigma	MABE50; RRID: AB_10807429
Anti-total SR Antibody (1H4)	Santa Cruz	sc-13509; RRID: AB_2185202
FITC anti-human CD45	BioLegend	368507; RRID: AB_2566367
APC anti-mouse CD45	BioLegend	103111; RRID: AB_312976
APC anti-human CD19	BioLegend	302211; RRID: AB_314241
APC anti-human CD3	BioLegend	300411; RRID: AB_314065
PE anti-human CD34	BioLegend	343605; RRID: AB_1732033
APC/Cyanine7 anti-human CD38	BioLegend	303533; RRID: AB_2561604
Anti-XIAP	Cell Signaling	2042S; RRID: AB_2214870
Anti-U2AF2	Abcam	ab37530; RRID: AB_883336
Anti-RBM5	Abcam	ab245646
Anti-MCL-1	SantaCruz	sc-12756; RRID: AB_627915
Anti-FLT3	Cell Signaling	3462S; RRID: AB_2107052
Bacterial and virus strains		
One Shot™ Stbl3™ Chemically Competent *E. coli*	Fisher	C737303
Chemicals, peptides, and recombinant proteins		
D-Luciferin, Potassium Salt	Gold-Bio Technology	Cat#LUCK-500
G418	ThermoFisher Scientific	10131027
Blasticidin	Fisher	Cat#A1113903
Polybrene	Sigma Aldrich	TR-1003-G
Polyethylenimine (PEI)	Polysciences, Inc	Cat#23966
Venetoclax	Fisher	NC1235948
SM09419	BioSplice	N/A
Cytarabine	Sigma	BP383
Etoposide	Sigma	E1383-25MG
Idarubicin hydrocholoride	Sigma	I1656-10MG
Midostaurin	SelleckChem	S8064
5-Azacytidine	SelleckChem	S1782
Critical commercial assays		
RNeasy Plus Mini Kit	Qiagen	Cat#74136
MethoCult GF M3434	StemCell Technologies	Cat#03434
CellTiter-Glo Luminescent Cell Viability	Promega	G7572
NucleoSpin Blood XL	Takara	740950.1
Verso cDNA synthesis kit	ThermoFisher Scientific	AB1453B
Nano-Glo Dual Luciferase Reporter Assay	Promega	N1610
Z'-LYTE Kinase assay	ThermoFisher Scientific	PV3190
Phusion Flash High Fidelity PCR Master Mix	Fisher	F548L
KAPA Hyper Library Preparation Kit	Roche	KK8500

(*Continued on next page*)

Continued

REAGENT or RESOURCE	SOURCE	IDENTIFIER
Deposited data		
RNA-seq Raw data	This paper	GSE199161
RBM10 eCLIP data	This paper	GSE199161
Whole exome sequencing data on venetoclax sensitive and resistant MOLM-13 cells	This paper	GSE199161
CRISPR screen data	This paper	Table S1
List of differentially expressed genes in RBM10-deleted AML cells treated with venetoclax or DMSO	This paper	Table S3
List of differentially spliced events in RBM10-deleted AML cells treated with venetoclax or DMSO	This paper	Table S4
List of differentially expressed genes in SM09419-treated AML cells treated with venetoclax or DMSO	This paper	Table S5
List of differentially spliced events in SM09419-treated AML cells treated with venetoclax or DMSO	This paper	Table S6
BeatAML database	Tyner et al.[43]	https://www.nature.com/articles/s41586-018-0623-z
Experimental models: Cell lines		
Human: MOLM-13	DSMZ	ACC 554
Human: NKM-1	JCRB	IFO50476
Human: MV4-11	ATCC	CRL-9591
Human: THP-1	ATCC	TIB-202
Human: U937	ATCC	CRL-1593.2
Human: TF-1	ATCC	CRL-2003
Human: HEK293T	ATCC	CRL-1573
Experimental models: Organisms/strains		
NOD scid gamma	JAX	Cat#005557
NSG-S	JAX	Cat#013062
C57BL/6J	JAX	Cat#000664
Mx-1 cre transgenic mice	JAX	Cat#005673
Rbm10 conditional knockout	This paper	N/A
Biological samples		
Patient 1 PDX (bone marrow)	This paper	N/A
Patient 2 PDX (PBMCs)	This paper	N/A
Oligonucleotides		
sgRNAs and primers, see Table S1	This paper	N/A
Human pooled genome-wide sgRNA library (Brunello) sequences	Doench et al.[83]	Addgene: 73179
Recombinant DNA		
Lenti-Cas9 Blasticidin	Sanjana et al.[80]	Addgene: 52962
psPAX2	Gift from Didier Trono	Addgene: 12260
pVSVG	Gift from Didier Trono	Addgene: 12259
LRG2.1-GFP sgRNA vector	Tarumoto et al.[84]	Addgene: 108098
Software and algorithms		
FlowJo V8.7	TreeStar (BD Biosciences)	https://www.flowjo.com/
Prism 9.0	GraphPad	https://www.graphpad.com

(*Continued on next page*)

Continued

REAGENT or RESOURCE	SOURCE	IDENTIFIER
Living Image Software	Perkin Elmer	http://www.perkinelmer.com/product/li-software-for-spectrum-1-seat-add-on-128113
GSEA	Broad Institute	http://software.broadinstitute.org/gsea/
IGV	Broad Institute	http://software.broadinstitute.org/software/igv/
CRISPResso	Pinello et al.[85]	http://crispresso.pinellolab.partners.org/)
Trim_galore v0.6.4	Martin et al.[88]	https://github.com/FelixKrueger/TrimGalore
STAR v2.7.5	Dobin et al.[89]	https://github.com/alexdobin/STAR
samtools v1.9	Danecek et al.[90]	http://www.htslib.org/
deeptools v3.3.1	Ramírez, et al.[91]	https://github.com/deeptools/deepTools
subread v1.5.0	Liao et al.[92]	https://subread.sourceforge.net/
RSEM v1.2.4	Li and Dewey.[96]	https://github.com/deweylab/RSEM
Bowtie	Langmead et al.[97]	https://github.com/BenLangmead/bowtie
edgeR	Robinson et al.[98]	Bioconductor
TopHat v2.0.8b	Trapnell et al.[99]	https://ccb.jhu.edu/software/tophat/index.shtml
MISO v2.0	Katz et al.[95]	http://hollywood.mit.edu/burgelab/miso/
tidyverse	Wickham et al.[101]	Bioconductor
UpSetR	Conway et al.[102]	Bioconductor
GenomicRanges	Lawrence et al.[106]	Bioconductor
picard v2.6.0	Broad Institute	https://github.com/broadinstitute/picard
bamutils v0.5.7	Breese et al.[103]	https://ngsutils.org/modules/bamutils/
DEWSeq	Huppertz et al.[105]	Bioconductor
htseq-clip	Anders et al.[104]	https://github.com/EMBL-Hentze-group/htseq-clip/
IHW	Ignatiadis et al.[107]	Bioconductor
fgsea	Korotkevich et al.[108]	Bioconductor

RESOURCE AVAILABILITY

Lead contact

Further information and requests for resources and reagents should be directed to and will be fulfilled by the lead contact, Omar Abdel-Wahab (abdelwao@mskcc.org).

Material availability

All unique reagents generated in this study are available from the lead contact without restriction.

Data and code availability

- All bulk RNA-seq and eCLIP as well as whole-exome sequencing of venetoclax resistant MOLM-13 cells have been deposited at GEO (GSE199161) and are publicly available as of the date of publication which is listed in the key resources table. The Tyner et al., 2018 data used for this study can be found with the Accession number (dbGaP:phs001657).
- This paper does not report original code.
- Any additional information required to reanalyze the data reported in this paper is available from the lead contact upon request.

EXPERIMENTAL MODEL AND SUBJECT DETAILS

Cell lines and cell culture

All human leukemia cell lines were cultured in recommended media, typically RPMI medium with 20% FBS and 1% penicillin/streptomycin. TF-1 human AML cell line was cultured in RPMI 20% FBS, 1% penicillin/streptomycin and 2 ng/mL GM-CSF. HEK293T cells were grown in DMEM medium with 10% FBS and 1% penicillin streptomycin. Cell lines transduced with lentiviral Cas9 blasticidin (Addgene plasmid no. 52962)[80] were selected with blasticidin (Fisher) 48 hours after transduction. All transfections were performed in HEK293T cells using Polyethylenimine (PEI) reagent at 4:2:3 ratios of plasmid: pVSVG: pPax2 in OPTI-MEM solution. Viral

supernatant was collected 48 hrs and 72 hrs post-transfection. Spin infections were performed at room temperature at 1,800 RPM for 30 mins with polybrene reagent (1:2000 dilution) (Fisher Scientific). All cell lines were authenticated in-house by our Integrated Genomics Operation (IGO) core based on fragment and STR analysis.

Animals

8-10 weeks-old female and male C57BL/6 and *Mx1-Cre* mice were purchased from Jackson Laboratory. 8 weeks-old NOD scid gamma and NSG-S female mice were obtained from Jackson Laboratory. Mice were bred and maintained in individual ventilated cages and fed with autoclaved food and water at Memorial Sloan Kettering Animal Facility. All animal procedures were completed in accordance with the Guidelines for the Care and Use of Laboratory Animals and were approved by the Institutional Animal Care and Use Committees at MSKCC. All mouse experiments were performed in accordance with a protocol approved by the MSKCC Institutional Animal Care and Use Committees (13-04-003).

Human patient samples

Studies were approved by the Institutional Review Boards of Memorial Sloan Kettering Cancer Center and conducted in accordance with the Declaration of Helsinki protocol. Primary human de-identified AML samples derived from whole peripheral blood or BM mononuclear cells were utilized. Mutational genotyping of each sample was performed by the MSKCC IMPACT assay as described previously.[81,82] Cord blood was acquired from NY Blood Bank. Informed consent was obtained from all subjects to obtain the patient specimens used in the studies described. Patient 1 is a 62 year old male and patient 2 is a 85 year old male. Specimens were obtained as part of the Memorial Sloan-Kettering Cancer Center Institutional Review Board approved clinical protocol #16-171 to which all subjects consented. O.A-W is a participating investigator on this protocol.

METHOD DETAILS

CRISPR screen

250 million MOLM13 Cas9-expressing cells were transduced with the Brunello sgRNA library[83] at a low multiplicity of infection (~0.3) to obtain at least 500 cells per sgRNA (500X). Spin infections were performed at room temperature at 1,500 RCF for 90 mins with polybrene reagent (1:2000 dilution) (Fisher Scientific). On Day 4 post-transduction, GFP percentage was assessed to determine infection efficiency and sgRNA coverage (~300-500X). Remaining 300-500X cells were placed back into culture after each passage until 20 days post-transduction. At day 8 post-transduction, pooled sgRNA cells were treated with either DMSO (1%), cytarabine (50 nM), 5-azacytidine (3 uM), etoposide (400 nM), idarubicin (5 nM), midostaurin (25 nM) or venetoclax (25 nM). Genomic DNA (gDNA) extraction using NucleoSpin Blood XL, Maxi kit for DNA from blood (Takara) according to manufacturer's protocol. For pooled CRISPR screen analysis, sgRNAs were normalized using the formula (sgRNA read count/total read count) x CPM+1. Subsequently, normalized reads were then used to calculate $\log_2$ fold change (normalized read count drug treatment/normalized read count DMSO). CRISPR library amplifications were performed according to published study.[83] Competition assays were performed using MOLM-13 cells transduced with sgRNA or cDNA constructs and mixed with parental cells at fixed ratios followed by 4 days of treatment with either vehicle (DMSO) or venetoclax, and GFP percentages were analyzed using BD LSR Fortessa FlowCytometer. The RNA processing factor (genes in the "RNA processing" gene ontology term, GO:0006396) sgRNA $\log_2$ fold change distributions in cytarabine, 5-azacytidine, etoposide, idarubicin, and midostaurin were compared to venetoclax. Specifically, a two-sided F-test for equality of variances was used to assess if the drug:venetoclax ratios significantly deviated from 1. Variance ratios and the 95% confidence intervals were estimated using the stats R package. For individual sgRNA validations, sgRNAs were cloned into LRG2.1 vector.[84]

CRISPR indel analysis

To quantify the spectrum of indel mutations with RBM10 sgRNAs, we transduced MOLM-13 cells with sgRBM10 or sgRosa (non-targeting), followed by cell sorting of GFP+/sgRNA+ populations at day 4 and day 28 post-infection. Cells were then harvested for gDNA and PCR amplicon (~200 bp) was designed to flank the sgRNA recognition sequence. 200 ng of gDNA was amplified using 2× Phusion Master Mix. Sequencing libraries were prepared from amplicons with an average size of 200 bp. The reported concentration was 3-7 ng/μL, and 50 μL were used as input for the KAPA Hyper Library Preparation Kit (Kapa Biosystems KK8504) according to the manufacturer's instructions with 8 cycles of PCR. Barcoded libraries were pooled in equal volumes and run on MiSeq in a PE150 run, using the MiSeq Reagent Micro Kit v2 (300 Cycles) (Illumina). The average number of read pairs per sample was 203,000.

Indel analysis was performed using CRISPResso (http://crispresso.pinellolab.partners.org/).[85]

RNA-sequencing library preparation and sequencing

For cell line RNA sequencing (RNA-seq), RNA was extracted from MOLM13 cells using the Qiagen RNeasy extraction kit, according to the manufacturer's instructions. A minimum of 500 ng of high-quality RNA (as determined by Agilent Bioanalyzer) per replicate was used as input for library preparation. Poly(A)-selected, strand-specific (dUTP method) Illumina libraries were prepared by the Integrated Genomics Operation (IGO) at Memorial Sloan Kettering with a modified TruSeq protocol and sequenced on the Illumina HiSeq 2000 to obtain ~50-60M 2 × 101 bp paired-end reads per sample.

eCLIP library preparation

eCLIP studies were performed in duplicates by Eclipse Bioinnovations Inc (San Diego, www.eclipsebio.com) according to the published single-end enhanced CLIP protocol with the following modifications. For Rbm10 immunoprecipitation, 10% of IP samples and 1% of input samples were run on NuPAGE 4–12% Bis-Tris protein gels, transferred to PVDF membrane, probed with 1:1,000 of RBM10 antibody and 1:10,000 TrueBlot Anti Rabbit IgG (HRP) and imaged with C300 Imager for 1 min on normal settings using Azure Radiance ECL. Only the region from ~100 kDa to 180 kDa (protein size to 80 kDa above) was isolated during eCLIP. For RNA visualization, 10% of IP samples were run on NuPAGE 4–12% Bis-Tris protein gels, transferred to nitrocellulose membrane, visualized using the Chemiluminescent Nucleic Acid Detection Kit (cat. no. 89880) from Thermo Fisher Scientific and imaged with C300 Imager for 30 seconds on normal settings. For eCLIP preparation, 10 million MOLM-13 cells were UV crosslinked at 400 mJoules/cm2 with 254 nm radiation, and snap frozen. Cells were then lysed and treated with RNase I to fragment RNA as previously described. RBM10 antibody (A301-006A, Bethyl) was then pre-coupled to Protein G Dynabeads (Thermo Fisher), added to lysate, and incubated overnight at 4 deg C. Prior to immunoprecipitation, 2% of the sample was taken as the paired input sample, with the remainder magnetically separated and washed with lysis buffer only (as the standard high-salt eCLIP wash buffer gave poor immunoprecipitation yield). eCLIP was performed by excising the area from ~100 kDa to ~180 kDa. RNA adapter ligation, IP-western, reverse transcription, DNA adapter ligation, and PCR amplification were performed as previously described.

Whole-exome sequencing and targeted capture sequencing

For MSKCC-IMPACT, after PicoGreen quantification and quality control by Agilent BioAnalyzer, 100 ng of DNA were used to prepare libraries using the KAPA Hyper Prep Kit (Kapa Biosystems KK8504) with 8 cycles of PCR. 80-190 ng of each barcoded library were captured by hybridization in pools of 6-14 samples using the IMPACT (Integrated Mutation Profiling of Actionable Cancer Targets) assay[81] (Nimblegen SeqCap), designed to capture all protein-coding exons and select introns of 505 commonly implicated oncogenes, tumor suppressor genes, and members of pathways deemed actionable by targeted therapies. Captured pools were sequenced on a NovaSeq 6000 in a PE100 run using the NovaSeq 6000 S4 Reagent Kit (200 Cycles) (Illumina) producing an average of 540X coverage per sample. For exome capture and sequencing, after PicoGreen quantification and quality control by Agilent BioAnalyzer, 100 ng of DNA were used to prepare libraries using the KAPA Hyper Prep Kit (Kapa Biosystems KK8504) with 8 cycles of PCR. After sample barcoding, 500 ng of library were captured by hybridization using the xGen Exome Research Panel v2.0 (IDT) according to the manufacturer's protocol. PCR amplification of the post-capture libraries was carried out for 12 cycles. Samples were run on a NovaSeq 6000 in a PE100 run, using the NovaSeq 6000 S4 Reagent Kit (200 Cycles) (Illumina). Samples were covered to an average of 251X.

Western blotting

MOLM-13 Cas9-expressing cells were transduced with sgRNAs and harvested for protein on day 6 post-transduction. For SM09419, MOLM-13 cells were treated with varying concentrations of SM09419, and protein was harvested 48 h post-treatment. Lysate protein concentration was measured with the BCA reagent and 10-30 mcg was loaded per lane onto 4-12% NuPAGE^{TM} Bis-Tris protein gels. After transfer, PVDF membranes were probed with anti-RBM10 (Bethyl Laboratories), anti-Phosphoepitope SR proteins Antibody (clone 1H4, Millipore Sigma), total SR protein (Santa Cruz), anti-XIAP (Cell signaling), anti-MCL-1 (Cell signaling), anti-RBM5 (Abcam), anti-FLT3 clone 8F2 (Cell signaling), anti-U2AF2/U2AF65 (Abcam) and anti-BCL-2 (Abcam) at 1:1,000 and visualized by standard methods.

Colony-forming assays

Total bone marrow from *Mx1*-Cre WT and *Mx1*-Cre *Rbm10*$^{fl/y}$ mice were harvested and seeded at a density of 20,000 cells per replicate into cytokine-supplemented methylcellulose medium (MethoCult M3434, Stemcell Technologies). For SM09419 experiments, total bone marrow from C57BL/6 treated with 25 mg/kg SM09419 for 3 weeks were harvested and seeded as described above. Colonies propagated in culture were scored at day 7.

Annexin V assay

Apoptotic analysis was determined using APC Annexin V (BD Bioscience) and performed according to manufacturer's specifications and co-stained with 4′,6-Diamidino-2-Phenylindole, Dihydrochloride (DAPI) for DNA content. Cells were analyzed by flow cytometry and FlowJo software.

Generation of Rbm10 conditional knockout mice

The Rbm10 allele was deleted by targeting exon 4. Two LoxP sites flanking exon 3 and a Frt flanked neomycin selection cassette were inserted in the downstream intron. Ten micrograms of the targeting vector were linearized and then transfected by electroporation of HF4 (129/SvEv x C57Bl/6) (FLP Hybrid) embryonic stem cells. After selection with G418 antibiotic, surviving clones were expanded for PCR analysis to identify recombinant ES clones. The Neo cassette in targeting vector has been removed during ES clone expansion. Screening primer A1 was designed downstream of the short homology arm (SA) outside the 3' region used to generate the targeting construct. Clones 182, 184, 211, 212, and 284 were expanded and reconfirmed for SA integration. A PCR was performed on clones 182, 184, 211, 212, and 284 to detect presence of the distal LoxP site using the LOX1 and SDL2 primers. This reaction amplifies a wild-type product 472 bp in size. The presence of a second PCR product 48 bp greater than the wild-type

product indicates a positive LoxP PCR. Confirmation of distal LoxP retention was performed by PCR using the LOX1 and FRTN2C primers. This reaction produces a product 1.05 kb in size. Sequencing was performed on purified PCR DNA to confirm presence of the distal LoxP cassette using the SDL2 primer. Secondary confirmation of positive clones identified by PCR was performed by Southern Blotting analysis. DNA was digested with Apa I, and electrophoretically separated on a 0.8% agarose gel. After transfer to a nylon membrane, the digested DNA was hybridized with a probe targeted against the 5' external region. DNA from HF4 mouse ES cells was used as a wild-type control. Positive clones were further confirmed by Southern Blotting analysis using an internal probe. DNA was digested with BamH I, and electrophoretically separated on a 0.8% agarose gel. After transfer to a nylon membrane, the digested DNA was hybridized with a probe targeted against the 3' internal region. DNA from HF4 mouse ES cells was used as a wild-type control. Primer set NDEL1 and NDEL2 was used to screen mice for the deletion of the Neo cassette. The PCR product for the wild-type is 322 bp. After Neo deletion, one set of LoxP-FRT sites remains (147 bp). A second band with a size of 469 bp indicates Neo deletion. A PCR was performed to detect presence of the distal LoxP site using the LOX1 and SDL2 primers. This reaction amplifies a wild-type product 473 bp in size. The presence of a second PCR product 48 bp greater than the wild-type product indicates a positive LoxP PCR. Tail DNA samples from positive mice were amplified with primers NEOGT and A1. NEOGT is located inside the Neo cassette and A1 is located downstream of the short homology arm, outside the region used to create the targeting construct. NEOGT/A1 amplifies a fragment of 2.32 kb in length.

Bone marrow (BM) transplantation

Freshly dissected femora and tibiae were isolated from *Mx1*-cre WT and *Mx1*-cre *Rbm10*$^{fl/y}$, CD45.2^{+} mice. BM was flushed with a 3-cc insulin syringe into PBS supplemented with 3% fetal bovine serum. The BM was spun at 0.5 g by centrifugation and RBCs were lysed in ammonium chloride-potassium bicarbonate lysis buffer for 5 min. After centrifugation, cells were resuspended in PBS plus 3% FBS, passed through a cell strainer, and counted. Finally, 0.5 million total BM cells of *Mx1*-cre WT and *Mx1*-cre *Rbm10*$^{fl/y}$ CD45.2^{+} mice were mixed with 0.5 million WT CD45.1^{+} support BM and transplanted via tail vein injection into lethally irradiated (two times 450 cGy) CD45.1^{+} recipient mice. Chimerism was measured by FACS from the peripheral blood 4 weeks after transplant. Chimerism was followed via FACS in the peripheral blood every 4 weeks (week 0, 4, 6, 8,12, and 16 after polyI:polyC injection). For noncompetitive transplantation experiments, 1 million total BM cells of *Mx1*-cre WT and *Mx1*-cre *Rbm10*$^{fl/y}$ CD45.2^{+} mice were injected into lethally irradiated (two times 450 cGy) CD45.1^{+} recipient mice.

Drug treatment IC_{50} measurements

Cell lines were plated in 96 well plates and exposed to the indicated compounds at various concentration ranges with a minimum of three technical replicates per concentration per cell line. Cell viability was measured with the CellTiter Glo reagent (Promega) as per manufacturer's instructions. Absolute viability values were converted to percentage viability versus DMSO control treatment, and then non-linear fit of log(inhibitor) versus response (three parameters) was performed in GraphPad Prism v7.0 to obtain an IC_{50} values. Two-dimensional heatmaps of Synergy Scores from Bliss synergy models were generated based on Demidenko et al., 2019.[86]

QPCR measurement of BCL2A1 gene expression

RNA was extracted from the indicated cell lines and reverse transcribed into cDNA using the Verso cDNA synthesis Kit (ThermoFisher Scientific). Measurement of *BCL2A1* gene expression was performed using primers amplifying *BCL2A1* CDS region and designed by primer3 (https://bioinfo.ut.ee/primer3-0.4.0/) with *ACTB* as the housekeeping gene. Relative expression levels across cell lines were calculated using the Delta-delta Ct method as per standard procedures.

cDNA overexpression

BCL2A1, *RBM10* wild-type and RBM10 domain mutants as well as XIAP full-length and Δexon 1 were codon optimized and synthesized as gene blocks by Integrated DNA Technologies (IDT) and was sublconed cloned into lentiviral Puro-IRES-GFP construct using NEBuilder Hifi DNA assembly. MOLM-13 RBM10-KO cells were transduced with either *BCL2A1*, *RBM10* wild-type, or *RBM10* mutant constructs and treated with venetoclax.

Animal experiments

For *in vivo* Cas9 experiments, MOLM-13 Cas9-expressing cells were transduced with sgRosa (negative control) or sgRBM10 constructs. At day 2 post-transduction, sgRNA positive cells (GFP^{+}) were sorted by FACS. 100,000 leukemia-sgRNA expressing cells were intravenously injected into each sub-lethal irradiated (5.5 Gy) 8 weeks-old NOD scid gamma mice mice. For venetoclax trials, a 100 mg/mL venetoclax (Sigma Aldrich) stock was diluted in a carrier containing 10% ethanol, 30% polyethyleneglycol-400 (Sigma), and 60% phosal 50 propylene glycol (Lipoid) to obtain a final concentration of 100 mg/kg. Upon disease onset as measured by bioluminescent imaging, we performed oral gavage once daily with either 100 mg/kg venetoclax or vehicle (1% DMSO). All whole-body bioluminescent imaging was performed by intraperitoneally injection of Luciferin (Goldbio) at a 50 mg/kg concentration and imaging was performed after 5 mins using an IVIS imager. Bioluminescent signals (radiance) were quantified using Living Image software with standard regions of interests (ROI) rectangles.

Kinase assays

IC_{50} values for CLK2, CLK3, DYRK1A and CDK1 were determined by transferring test compounds to 1536-well plates (Echo 550, LabCyte) and by optimizing and performing Z'-LYTE™ kinase assays per the manufacturer's instructions (Thermo Fisher). In addition, a full kinome screen (464 kinases) with 1 μM SM09419 was performed by Thermo Fisher Select Screen service. The IC_{50} for each kinase demonstrating >80% inhibition was then determined. Kinase tree dendrogram was generated using Coral.[87]

NanoBRET target engagement assay

Cellular target engagement assays were performed using NanoBRET in 293T cells expressing CLK1, CLK2, CLK3, CLK4, DYRK1A, DYRK1B, and DYRK2 in-frame with a nanoluciferase (NanoLuc) tag. A cell permeable NanoBRET fluorescent tracer was then added to the cells which reversibly binds the target-NanoLuc Fusion protein in live cells to result in a BRET signal. SM09419 or vehicle were then added to each cell over a dose range and the degree of drug-target protein binding was assessed via loss of NanoBRET signal. An IC_{50} value indicating SM09419-protein binding was then identified via 10-point dose response curves.

Patient-derived xenograft experiments

Frozen human peripheral blood mononuclear cells (PBMCs) from two individual PDX models were rapidly thawed and transferred into 50 mL conical tubes. 20 mL pre-warmed RPMI 1640 (Corning) was added dropwise to tubes. After centrifuging at 300 × g at 4 degrees Celsius, cell pellet was resuspended in PBS (Corning). 4 million cells were intrafemorally injected per mouse. Blood was collected by retro-orbital bleeding using heparinized microhematocrit capillary tubes (Thermo Fisher Scientific) and a flow cytometry panel consisting of mCD45/ hCD45/hCD3/hCD11b/hB220 were used to discriminate human from mouse cells and human myeloid vs T-cell engraftment. Upon disease onset as measured by hCD45-positive cells by flow cytometry, we performed oral gavage once daily with either 25 mg/kg SM09419 or vehicle (5% polyvinylpyrrolidone).

QUANTIFICATION AND STATISTICAL ANALYSIS

Genome-wide differential gene expression analysis

FASTQ files were first trimmed using Trim_galore (v0.6.4)[88] to remove sequencing adapters and low quality (Q<15) reads. Trimmed sequencing reads were aligned to the human Hg19 reference genome (GENCODE, GRCh37.p13) using STAR (v2.7.5).[89] SAM files were subsequently converted to BAM files, sorted, and indexed using samtools (v1.9).[90] BAM files were used to generate bigwig files using bamCoverage (part of the Deeptools package; v3.3.1).[91] Read counting across genomic features was performed using featureCounts (part of the subread package; v1.5.0).[92]

Gene expression estimation and alternative splicing analysis

Annotations from UCSC knownGene,[93] Ensembl 71,[94] and MISO v2.0[95] were combined to create a genome annotation for the human UCSC hg19 (GRCh37) assembly. We mapped all reads to the transcriptome via RSEM v1.2.4,[96] using the Bowtie alignment option "-v 2".[97] RSEM produces gene-level estimates of expression in units of transcripts per million (TPM). All gene expression estimates were normalized via the trimmed mean of M values (TMM) method.[98] Reads which failed to align were mapped to the genome with TopHat v2.0.8b,[99] as well to an expanded annotation created by computing all possible combinations of annotated 5′ and 3′ splice sites per gene. We quantified isoform expression with MISO v2.0,[95] using the combined RSEM and TopHat alignments as input. We used the two-sided t-test to test differential isoform expression between sample groups. Differentially spliced events were defined as those with at least 20 isoform-identifying reads in each sample, a minimum absolute difference of 10% in isoform expression, and a p-value < 0.05. All analyses were conducted within the R Programming environment with tools from Bioconductor.[100] The visualizations were created using the dplyr, ggplot2, tidyverse,[101] and UpSetR[102] packages.

Purine/Pyrimidine motif enrichment analysis

Differentially spliced cassette exon events following SM09419 treatment were identified. The enrichment of purines/pyrimidines in excluded, relative to included, cassette exons was measured within exonic regions and immediately adjacent intronic sequences. The 95% confidence interval was estimated with bootstrapping (1000 resampling iterations). The motif enrichment analysis was conducted within the R Programming environment with GenomicRanges from Bioconductor.[100]

eCLIP data analysis

The eCLIP data was processed similarly as described previously[37] and is outlined shortly in the following. First, adapter sequences were trimmed from both reads of all read-pairs using cutadapt version 1.14. Then, all remaining reads longer than 16 bases were aligned against the human reference genome sequence hg19/GRCh37 using STAR version 2.5.0c. Only uniquely mapped reads were kept. Read-pair duplicates by position were removed using picard tools version 2.6.0. To identify binding sites, we first ran a custom script to identify clusters of overlapping reads that had a read-depth of at least 10 reads. Then, we calculated significant enrichments for all such identified clusters by comparing IP-samples versus input-samples using edgeR. More specifically, we ran bamutils count version 0.5.7[103] to counted stranded reads within all identified clusters for all samples. Using this output, we calculated differential coverage between IP-vs-input for each cluster with edgeR after normalizing for total sequencing depth per replicate (resulting in counts per million/CPM per cluster). Final binding sites were called by applying logFC > 2 and FDR < 0.05 thresholds

between IP-vs-input. Identification of RBM10 binding positions in events alternatively spliced following RBM10 KO relied on the htseq-clip suite (https://htseq-clip.readthedocs.io),[104] and the DEWSeq[105] and GenomicRanges Bioconductor packages.[106] In brief, the GRCh38.v40 GENCODE annotation was processed into 50 nucleotide (nt) genomic sliding windows, with step size of 20 nt, using htseq-clip. From the STAR-aligned eCLIP BAM files, htseq-clip was used to identify crosslink positions and count their abundance in each window. The htseq-clip counts matrix was used as input to DEWSeq for normalization and identification of IP-vs-input significantly enriched windows (adjusted p-value < 0.05, logFC > 2) in protein-coding regions. The p-values were FDR-adjusted via Independent Hypothesis Weighting[107] and overlapping significantly enriched windows were combined. The positions of enriched windows in alternatively spliced regions identified from our RNA-seq analyses were determined using the GenomicRanges package.

Gene ontology analysis

Gene set enrichment was performed using the fgsea R package (1.4.0)[108] using the KEGG, GO and MsigDB specific signatures according to the manual.

Statistical analysis

Kaplan-Meier survival curve p-values were performed using Log rank Mantel-COX test. For statistical comparison, we performed unpaired Student's t test. Statistical analyses were performed using Prism 7 software (GraphPad). Data with statistical significance are as indicated, *p< 0.05, **p< 0.01, ***p< 0.001. Kaplan-Meier survival curves were compared using the Wilcoxon Rank-Sum test via GraphPad Prism. Information on replicates, independent experiments and statistical test can be found in the Figure Legends.